

OPEN ACCESS

**Repository of the Max Delbrück Center for Molecular Medicine (MDC)
in the Helmholtz Association**

<https://edoc.mdc-berlin.de/21390/>

**Hypothalamic galanin-producing neurons regulate stress in zebrafish
through a peptidergic, self-inhibitory loop**

Corradi L., Bruzzone M., Maschio M.D., Sawamiphak S., Filosa A.

This is the final version of the accepted manuscript. The original article has been published in final edited form in:

Current Biology
2022 APR 11 ; 32(7): 1497-1510
2022 FEB 25 (first published online: final publication)
doi: [10.1016/j.cub.2022.02.011](https://doi.org/10.1016/j.cub.2022.02.011)

Publisher: [Cell Press](#) / [Elsevier](#)



Copyright © 2022 Elsevier Inc. This manuscript version is made available under the [Creative Commons Attribution-NonCommercial-NoDerivatives 4.0 International License](http://creativecommons.org/licenses/by-nc-nd/4.0/). To view a copy of this license, visit <http://creativecommons.org/licenses/by-nc-nd/4.0/> or send a letter to Creative Commons, PO Box 1866, Mountain View, CA 94042, USA.

Hypothalamic Galanin-producing neurons regulate stress in zebrafish through a peptidergic self-inhibitory loop

Laura Corradi^{1,2}, Matteo Bruzzone³, Marco dal Maschio^{3,4}, Suphansa Sawamiphak^{1,5},
Alessandro Filosa^{1*}

Affiliations:

¹ Max Delbrück Center for Molecular Medicine in the Helmholtz Association (MDC), Berlin, Germany

² Freie Universität Berlin, Institute for Biology, Berlin, Germany

³ Padova Neuroscience Center, Università degli Studi di Padova, Padua, Italy

⁴ Department of Biomedical Sciences, Università degli Studi di Padova, Padua, Italy

⁵ DZHK (German Center for Cardiovascular Research), Partner Site Berlin, Berlin, Germany

* Correspondence: Alessandro.Filosa@mdc-berlin.de

Summary

Animals possess neuronal circuits inducing stress to avoid or cope with threats present in their surroundings, for instance by promoting behaviors such as avoidance and escape. However, mechanisms must exist to tightly control responses to stressors, since overactivation of stress circuits is deleterious for the wellbeing of an organism. The underlying neuronal dynamics responsible for controlling behavioral responses to stress have remained unclear. Here we describe a neuronal circuit in the hypothalamus of zebrafish larvae that inhibits stress-related behaviors, and prevents excessive activation of the neuroendocrine pathway hypothalamic-pituitary-interrenal axis. Central components of this circuit are neurons secreting the neuropeptide Galanin. Ablating these neurons led to abnormally high levels of stress, while activating them reduced stress. Surprisingly, we found that Galanin has a self-inhibitory action on Galanin-producing neurons. Our results suggest that hypothalamic Galanin-producing

neurons play an important role in fine-tuning stress responses by preventing potentially harmful overactivation of stress-regulating circuits.

Key words: Stress, Zebrafish, Behavior, Neuronal Circuits, Galanin, Hypothalamus

Introduction

Stress is an internal state capable of strongly influencing animal behavior. Neuronal circuits regulating stress evolved to help animals to cope with adverse environmental conditions by promoting adaptive responses essential for survival, such as avoidance of potential threats.¹⁻³ The same circuits, when not functioning properly, can also induce emergence of maladaptive behaviors.⁴ In humans, dysregulation of stress circuits leads to several debilitating psychiatric conditions, including post-traumatic stress disorder, depression, and occupational burnout.⁴⁻⁷ Collectively, stress-related pathologies represent a great burden for individuals and society. A better understanding of functioning of neuronal networks controlling stress would not only advance our knowledge of the circuits regulating internal states, but also potentially contribute to the development of new therapeutic strategies to treat mental illness.

The hypothalamus is a brain region centrally involved in controlling physiological and behavioral responses to stress. For example, the hypothalamic-pituitary-adrenal (HPA) axis is a major stress-regulating neuroendocrine pathway.^{4,8,9} Activation of the HPA axis starts with extrinsic (sensory) and intrinsic (homeostatic) signals converging on neurons producing corticotropin-releasing hormone (Crh) in the hypothalamus, and culminates with the release of cortisol by the adrenal gland, triggered by adrenocorticotrophic hormone (Acth) secreted from the pituitary gland. Although the HPA axis is essential to initiate physiological alterations in the brain and peripheral organs to allow proper responses to stressful conditions,^{4,8} if left unchecked its activity is harmful to an animal's wellbeing.^{4,6} Therefore, tightly regulated systems must exist to control proper activation of the HPA axis and other circuits promoting stress to ensure that they are engaged in the presence of potentially dangerous threats, and disengaged once safe conditions are reestablished. One of such control systems is a negative

feedback mediated by cortisol, which dampens activity of the HPA axis, mostly through regulation of gene transcription.^{8,10} However, since this negative feedback system is relatively slow,^{9,11} neuronal circuits for fast modulation of stress are required to quickly and dynamically regulate stress in response to sensory information.^{11,12}

A large portion of the neurons regulating responses to stressors secretes neuropeptides, such as arginine-vasopressin, oxytocin, Crh, Galanin (Galn), and Neuropeptide Y,^{11,13} but our understanding of functioning of the neuronal circuits mediating the action of these neuropeptides is still limited. For example, Galn has been implicated in anxiety disorders, depression, substance abuse, and other pathological states related to stress.^{14,15} However, the mechanisms by which Galn mediates the impact of stress on neuronal circuits and behavior are largely unknown. Here we discovered that a small genetically-labelled hypothalamic population of neurons producing the neuropeptide Galn regulates responses to stressors in larval zebrafish, a model organism with a small and translucent brain well suited for studying the hypothalamic circuits regulating stress, owing to the possibility to easily image and manipulate activity of genetically identified neurons.¹⁶⁻²⁰ Importantly, the neuronal circuits and molecular pathways regulating stress in zebrafish are very similar to the ones present in mammals.^{21,22} For example, the fish hypothalamic-pituitary-interrenal (HPI) axis is anatomically and functionally similar to the mammalian HPA axis.^{21,23} Moreover, zebrafish has been used as a model to study the neurobiology of stress and stress-related psychiatric conditions.²⁴⁻²⁷

We found that a subpopulation of hypothalamic Galn-producing (Galn⁺) neurons is a key negative regulator of stress, since their removal exacerbates activation of the HPI axis and motor responses to stressors. Surprisingly, we also found that these cells do not use Galn to communicate with downstream neurons controlling stress-related motor behavior. Instead, the neuropeptide reduces activation of neurons producing it. Finally, we show that Galn⁺ neurons inhibit activity of Crh⁺ neurons, which are centrally involved in the activation of the HPI axis, likely through GABAergic transmission.

Taken together, our data shed new light on the mechanisms underlying the action of a discrete genetically-labeled hypothalamic microcircuit, which prevents potentially deleterious overactivation of a stress-promoting neuroendocrine pathway.

Results

A population of Galn⁺ neurons in the preoptic area is activated by stressful stimuli

To understand the role of Galn⁺ neurons in regulating responses to stress, we took advantage of a transgenic line expressing the gene encoding the transcription factor Gal4 under the control of the *galn* gene regulatory sequences, labeling a small group of neurons in the zebrafish hypothalamus²⁸ (Figure 1A, S1). Two clusters of cells are genetically labeled in this line at 5 days post fertilization (dpf): an anterior population in the preoptic area (PoA), and a second one in the posterior region of the hypothalamus (pHyp) (Figure 1A, S1).

To test whether Galn⁺ neurons are activated by stressors, we exposed 5 dpf *galn:Gal4; UAS:EGFP* larvae to a hypertonic solution (100 mM NaCl), a well characterized stressor for zebrafish,²⁹ and measured neuronal activation by detecting amounts of phosphorylated Extracellular signal-Regulated Kinase (pERK) protein in Galn⁺ neurons (Figure 1B). Intensity of pERK immunofluorescence staining was shown to be a reliable proxy of activity of zebrafish neurons.³⁰ We found that Galn⁺ neurons in the PoA of larvae exposed to the hypertonic solution displayed an increase of neuronal activity, measured as pERK/total ERK (tERK) ratio, compared to Galn⁺ neurons in control larvae (Figure 1C), suggesting that at least a portion of Galn⁺ neurons are activated in the presence of a stressor. On the contrary, in the pHyp we observed overall lower pERK/tERK values in Galn⁺ neurons in larvae exposed to the hypertonic solution compared to controls (Figure 1D), suggesting that the function of Galn⁺ cells in responding to stressors may differ between the pHyp and the PoA. pERK/tERK values in randomly selected Galn-negative neurons in the telencephalon were not altered by the administration of the hypertonic solution (Figure S2), indicating that the stressor induced specific changes of activity in Galn⁺ neurons that were not due to generalized alterations of

neuronal activity in the brain. To prove that Galn⁺ neurons are sensitive to stressors in general rather than only to osmolarity changes, we exposed 5 dpf *galn:Gal4; UAS:EGFP* fish to bright blue light (Figure S3), a stimulus previously shown to induce stress in zebrafish larvae.³¹ Galn⁺ neurons in the PoA of fish exposed for five minutes to flashing blue light (470 nm) displayed higher pERK/tERK values compared to controls (Figure 1E), confirming that they are sensitive to different types of stressors. On the contrary, Galn⁺ cells in the pHyp were not responsive to blue light (Figure 1F), suggesting that their activity may be regulated by osmotic changes rather than stressful stimuli in general.

Subpopulations of Galn⁺ neurons display heterogenous stressor-induced response profiles

To better characterize the dynamics underlying responses to stressors of Galn⁺ neurons we performed calcium imaging in 5 dpf *galn:Gal4; UAS:GCaMP6s* larvae (Figure 2A) exposed to the 100 mM NaCl solution while being embedded in agarose. These experiments revealed a more complex scenario compared to the pERK/tERK data. Interestingly, while we confirmed that the majority of Galn⁺ neurons in the PoA are activated by the hypertonic solution, we also discovered subpopulations of neurons with different response profiles (Figure 2B, C, S4A). Overall, we observed four different types of response: increased activity (1) or decreased activity (2) after exposure to the hypertonic solution, and lack of response in neurons either active (3, defined as non responsive) or inactive (4) before and after application of the hypertonic solution (Figure 2B – E). The response profiles of Galn⁺ neurons were reproducible across trials. Indeed, when fish were exposed twice to the hypertonic solution, we observed similar percentages of the four neuronal types in the two trials (Figure S5A, B). Moreover, the majority of neurons were classifiable as the same type of response profile when the hypertonic solution was applied a second time (Figure S5C). Furthermore, comparison of the firing patterns of each neuron in the two trials showed that they had a positive average Pearson correlation coefficient, which was significantly higher than the mean Pearson coefficient of randomly matched neurons across trials (Figure S5D), confirming reproducibility of the

responses. In contrast, percentages of the four categories were starkly different following application of a control saline solution, with the majority of Galn⁺ neurons belonging to either the “non responsive” or “inactive” types (Figure S5E – H). Anatomical analysis of the localization of the imaged cells revealed that the different subpopulations of Galn⁺ neurons in the PoA do not appear to be organized in spatially segregated clusters, but are instead evenly distributed within this brain region (Figure 2F, G). Moreover, we did not detect any evident trend in the comparison between correlation of activity (Pearson correlation coefficient) and physical distance between Galn⁺ neurons, further suggesting that different functional types of Galn⁺ neurons are not organized in spatial subdomains (Figure 2H).

We also observed the four categories of responses in Galn⁺ neurons in the pHyp (Figure S4B – F). However, in this brain region more Galn⁺ neurons were inactive or displayed reduced activity after exposure to the stressor, compared to neurons in the PoA, in accord with our previous results showing lower pERK/tERK values in these neurons (Figure 1D).

Taken together, these data indicate that Galn⁺ neurons in the zebrafish brain belong to different subpopulations differentially affected by the presence of a stressor, and that the main population activated by aversive stimuli resides in the PoA.

Galn⁺ neurons in the PoA are required for proper behavioral responses to stress

The observation that activity of Galn⁺ neurons changes in response to application of stressors prompted us to test whether their presence is required for regulating stress-related behavioral responses. To this end, we performed a behavioral test to measure locomotor changes after exposure to the hypertonic solution, which leads to increased motility in zebrafish larvae,³² thus serving as a readout of stress levels (Figure 3A). We ablated Galn⁺ neurons by using a chemogenetic approach employing the genetically-encoded enzyme nitroreductase (NTR)³³ and the drug nifurpirinol.³⁴ The NTR in *galn:Gal4; UAS:NTR-mCherry* larvae, converts nifurpirinol in a toxic compound killing Galn⁺ neurons. Ablation of Galn⁺ cells did not alter spontaneous locomotion of larvae (Figure 3B), indicating that it does not have generalized negative effects on motor behavior. However, we observed that fish lacking Galn⁺

cells displayed an elevated behavioral response to the hypertonic solution, compared to control non-ablated larvae (Figure 3C, D). Moreover, fish without Galn⁺ neurons had higher amounts of cortisol compared to control larvae after exposure to the hypertonic solution (Figure 3E), strongly suggesting that the increased motor activity in response to the stressor is directly linked to elevated activation of the HPI axis in fish lacking Galn⁺ cells. Furthermore, compared to controls, larvae in which Galn⁺ neurons were ablated showed elevated acoustic startle response probability (Figure 3F), a phenotype often associated with stress and anxiety-like states.³⁵⁻³⁷

The fact that the hyperosmotic stressor mostly activated Galn⁺ neurons in the PoA, in contrast to a minority of neurons in the pHyp, prompted us to test whether they alone are required for proper behavioral responses to stress. To this end, we performed two-photon-laser-mediated ablations of Galn⁺ cells in the PoA (Figure 3G), leaving intact neurons in the pHyp. The ablation procedure did not cause generalized motor defects, since 5 dpf *galn:Gal4; UAS:EGFP* ablated larvae displayed normal spontaneous locomotion (Figure 3H). Importantly, ablating Galn⁺ neurons in the PoA was sufficient to cause increased behavioral responses to the hypertonic solution (Figure 3I, J), suggesting that these neurons are important regulators of stress responses in zebrafish.

Lack of Galn reduces behavioral responses to stress, and its overexpression increases them

To test whether the peptide Galn mediates the stress-modulatory function of Galn⁺ neurons, we used the CRISPR/Cas9 technique to generate a *galn* mutant (*galn^{md76}*) harboring a 11 base pair deletion in exon 3 of the gene encoding Galn (Figure 4A), causing a frameshift mutation and creation of a premature stop codon. Immunostaining with an anti-Galn antibody showed absence of the peptide in 5 dpf *galn^{md76/md76}* larvae (Figure 4B). Spontaneous locomotion was not altered in 5 dpf *galn^{+/md76}* and *galn^{md76/md76}* larvae (Figure 4C), suggesting that the mutation does not cause generalized motor impairments. Next, we measured motility changes in 5 dpf *galn^{+/+}*, *galn^{+/md76}*, and *galn^{md76/md76}* larvae exposed to the 100 mM NaCl hypertonic solution.

We found that *galn*^{md76/md76} larvae displayed reduced motility after application of the stressor, compared to *galn*^{+/+} and *galn*^{+/md76} fish (Figure 4D, E). Accordingly, overexpressing *galn* specifically in Galn⁺ neurons, by injecting a plasmid containing an *UAS:galn-T2A-tdTomato-CAAX* construct in single-cell-stage *galn:Gal4* embryos (Figure 4F, G), increased behavioral stress responses after exposure to the hypertonic solution (Figure 4H, I), without altering spontaneous locomotion in the absence of the stressor (Figure 4J). The phenotypes of the *galn*^{md76} mutants and the *galn*-overexpressing fish are surprising, since they are opposite to what we expected based on the phenotype of larvae lacking Galn⁺ neurons, which displayed elevated responses to stress (Figure 3). Taken together, our behavioral data suggest that Galn is not the neurotransmitter mediating stress-related signaling downstream of Galn⁺ neurons.

Lack of Galn increases stressor-induced activation of Galn⁺ neurons in the PoA

Interestingly, we found that similarly to Galn⁺ neurons in the PoA of mice,³⁸ the vast majority of Galn⁺ neurons in the PoA of 5 dpf zebrafish larvae are GABAergic (Figure 5A, B), since they express the gene *glutamate decarboxylase 2 (gad2)*, encoding an enzyme required for the synthesis of GABA. Moreover, by using fluorescence *in situ* hybridization chain reaction (HCR),³⁹ we found that a large fraction of Galn⁺ cells in the PoA express at least one of three genes encoding Galn receptors (*galnR1a*, *galR1b*, *galnR2b*) (Figure 5C – F). We did not detect expression of the fourth Galn-receptor-encoding gene *galnR2a* in Galn⁺ neurons (Figure 5E, F). These results led us to hypothesize that Galn⁺ neurons might use GABA to communicate with downstream cells, while Galn may have an inhibitory action on Galn⁺ neurons (Figure 6A). According to this model, lack of Galn in *galn*^{md76/md76} fish would increase activity of Galn⁺ neurons, which in turn would enhance the inhibitory action on downstream stress-promoting neurons, and consequently cause decreased behavioral responses to stress, as shown in Figure 4D, E. To prove this hypothesis, we performed calcium imaging of Galn⁺ neurons in the PoA of 5 dpf *galn:Gal4; UAS:GCaMP6s; galn*^{md76/md76} larvae (Figure 6B – D, S6A). Lack of Galn did not substantially alter proportions of response types in Galn⁺ neurons (Figure 6B), but increased the frequency of calcium events in neurons of the “increased activity” type before

and after addition of the hypertonic solution (Figure 6C). Activity of neurons of the “decreased activity” type was not significantly altered (Figure 6D). To further prove the presence of an autoinhibitory effect of Galn on Galn⁺ neurons, we overexpressed *galn* in Galn⁺ cells by injecting the plasmid containing the *UAS:galn-T2A-tdTomato-CAAX* sequence in *galn:Gal4; UAS:GCaMP6s* embryos at the single-cell stage, and measured stressor-induced activation of Galn⁺ neurons at 5 dpf (Figure 6E – G, S6B). Percentages of the four classes of neurons were similar in fish injected with *galn*-overexpressing or control (*UAS:tdTomato-CAAX*) plasmids (Figure 6E). In accord with our hypothesis, increasing expression of *galn* in Galn⁺ cells reduced the frequency of calcium events in neurons of the “increased activity” type after application of the hypertonic solution (Figure 6F), without altering activity of “decreased activity” neurons (Figure 6G). Taken together, these data strongly suggest that Galn has an inhibitory action on a subpopulation of Galn⁺ neurons, possibly through an autocrine mechanism.

Galn⁺ neurons negatively modulate activity of Crh⁺ cells in the PoA

Our results revealed an important role for Galn⁺ neurons in regulating behavioral responses to stress and activity of the HPI axis. However, so far we have not identified the downstream cells mediating the action of Galn⁺ neurons on this neuroendocrine pathway. We hypothesized that Galn⁺ neurons could inhibit Crh⁺ neurons in the PoA, the principal activators of the HPI axis. To verify this possibility, we first monitored with calcium imaging the activity of Galn⁺ and Crh⁺ neurons in the PoA before and after exposure to 100 mM NaCl (Figure 7A, S7). Galn⁺ cells in 5 dpf *galn:Gal4; UAS:NTR-mCherry; elavl3:H2B-GCaMP6s* larvae were identifiable during live imaging by expression of *NTR-mCherry*. Crh⁺ neurons were identified *post mortem* by detecting *crhb* mRNA with fluorescence *in situ* HCR, and by aligning to a reference brain the image stacks of the fixed samples and the ones obtained during live imaging of the same fish (see Star Methods for details). We observed the presence of several types of stressor-induced responses not only in Galn⁺ neurons, but also in Crh⁺ ones, as previously reported²⁵ (Figure S7). We focused our attention on Galn⁺ neurons displaying stressor-induced increase of activity and their relation to Crh⁺ cells with either increased or decreased activity (Figure

7A). Interestingly, we detected negative cross-correlation between the activity of Galn⁺ neurons of the “increased activity” type and Crh⁺ cells with decreased activity after exposure to the stressor (Figure 7B), supporting our hypothesis of an inhibitory action of a subpopulation of Galn⁺ cells on Crh⁺ neurons. To further prove this hypothesis, we performed fluorescence *in situ* HCR to detect *crhb* mRNA, followed by immunofluorescence staining of pERK and tERK as a readout of neuronal activation (Figure 7C). In accord with previous results,²⁵ we found that application of 100 mM NaCl for two minutes led to activation of Crh⁺ neurons in the PoA of 5 dpf wild type larvae, as revealed by higher pERK/tERK values compared to fish exposed to a control solution (Figure 7D). Importantly, stressor-induced activation of Crh⁺ neurons was higher in 5 dpf larvae lacking Galn⁺ neurons (*galn:Gal4; UAS:NTR-mCherry* fish treated with nifurpirinol) than in unablated control fish (treated with nifurpirinol, but lacking *NTR-mCherry* expression) (Figure 7E). Interestingly, we found that activation of Crh⁺ neurons was elevated also in the absence of the hypertonic solution (Figure 7F), suggesting that Galn⁺ neurons are upstream regulators of Crh⁺ cells, negatively controlling their activation not only in the presence of stressors, but also in basal conditions.

Discussion

Neuronal circuits regulating stress are essential to initiate behavioral and physiological responses that allow neutralization of environmental threats. However, mechanisms must exist to tightly control activation and inactivation of stress circuits, since a prolonged state of stress is deleterious. A better understanding of the functioning of these circuits is important not only for improving our knowledge about neuronal regulation of internal states, but also for potential clinical applications. We were able to pinpoint a small population of neurons producing the neuropeptide Galn in the PoA, which acts as a brake on stress induction. Majority of these neurons are quickly activated by stressors, and their ablation leads to abnormally elevated stress-related behavior.

We identified two main populations of Galn⁺ neurons in the hypothalamus of zebrafish, and discovered a remarkable diversity in terms of their responses to stressors. First, we observed

a major difference between the PoA and the pHyp clusters. Indeed, while the former appears to contain neurons responding to different types of stressors, neurons in the pHyp are responsive to osmotic changes, but not to intense light stimuli. These data suggest that Galn⁺ neurons in the PoA act as general detectors of stressors, in agreement with previous studies showing that the preoptic region of the zebrafish brain is an important hub for processing stress-inducing stimuli.²³ Second, within the PoA cluster we identified four different subtypes of Galn⁺ neurons. The majority of them respond strongly to the presence of a stressor, fewer are inhibited by it, and still fewer of them are unresponsive (either active or silent during recording periods). This diversity of response profiles may, at least in part, explain the involvement of Galn⁺ neurons in different types of behaviors. For example, the unresponsive Galn⁺ neurons we observed may be required for behaviors not related to stress. Indeed, it was shown that hypothalamic neurons producing Galn can also regulate food intake,⁴⁰⁻⁴⁴ and parental behavior^{38,45} in rodents, and sleep in zebrafish.^{46,47} It would be interesting in the future to understand how different subpopulations of Galn⁺ neurons contribute to diverse behaviors, and if different behaviors can be modulated by the same neuronal subtypes. For example, it may be possible that the subpopulation of neurons responsive to stressors we identified here could also contribute to regulate sleep, a behavior that is strongly influenced by stress.⁴⁸

The fact that Galn⁺ neurons in the PoA can be activated by several types of stressors, including hypertonic solution and intense blue light, suggests that these neurons receive information from different sensory systems, including the visual system and brain regions relaying information about salinity, possibly involving olfactory circuits.⁴⁹ The different sensory modalities could either converge directly on the Galn⁺ cells, or on other neurons directly or indirectly upstream of them. Further work will be required to reveal the neuronal pathways linking sensory circuits to Galn⁺ neurons.

Our results also provide a better understanding of the function of the neuropeptide Galn in the regulation of stress. Previous work showed that Galn is involved in stress and stress-related neuropsychiatric conditions, such as anxiety and depression.^{14,15,50,51} However, knowledge about the mechanisms mediating the effect of Galn on stress regulation has been

very limited. Here we pinpointed a specific mode of action by which Galn regulates stress. We were surprised to observe that while ablation of Galn⁺ neurons caused increased stress-related motor behavior, mutation of the *galn* gene led to the opposite phenotype. These results suggest that Galn is not the neurotransmitter mediating the action of Galn⁺ cells on downstream stress-promoting neurons. Instead, by using calcium imaging methods, we found that lack of Galn increases the activity of Galn⁺ neurons in the PoA, suggesting that it has a self-inhibitory action on Galn⁺ neurons. This interpretation of our results is also supported by the fact that Galn⁺ neurons express genes encoding Galn receptors. Since the *galn*^{md76} is not an inducible mutant allele, we cannot completely rule out a contribution of developmental alterations to the phenotypes we observed. However, our data showing that *galn*^{md76/md76} fish display increased responsiveness of Galn⁺ neurons to a stressor, and reduced behavioral stress responses—phenotypes mirroring the ones present in larvae lacking Galn⁺ neurons, or in fish with Galn⁺ neurons overexpressing *galn*—strongly suggest a specific role of Galn in modulating stress.

We found that, like in mice,³⁸ Galn⁺ neurons in the PoA of zebrafish larvae are GABAergic. It is likely that these neurons use GABA to inhibit downstream stress-promoting neurons, while Galn controls excitability of Galn⁺ cells, and/or release of GABA from them. This hypothesis is supported by previous studies showing that Galn is capable of hyperpolarizing neurons and inhibiting release of several neurotransmitters.⁵²⁻⁵⁶ We showed that Galn⁺ neurons contain three different subtypes of GalnRs. We still do not know if all the subtypes or only some of them mediate the inhibitory action of Galn on Galn⁺ cells. In mammals, it was shown that GalnR1 inhibits neuronal activity,^{15,55} while GalnR2 appears to be able to have both inhibitory and excitatory effects on cells expressing it.^{15,55} Furthermore, it is still not clear if the zebrafish orthologues have conserved functions. Further work will be required to pinpoint precisely the receptor(s) and downstream signaling transduction mechanisms responsible for reducing activity of Galn⁺ neurons.

One of the major regulators of stress in vertebrates is the HPA/I axis.^{9,21} We observed that hypothalamic Galn⁺ neurons inhibit activation of the HPI axis, by acting on Crh⁺ neurons in the

PoA, which are key components of the neuronal circuits inducing stress. This inhibitory effect could be mediated by direct inhibitory synapses between Galn⁺ and Crh⁺ neurons, or through the action of intermediary neurons. These results enrich our understanding of the complex neuronal networks modulating the activity of this important neuroendocrine pathway.

Taken together, our results suggest a model in which Galn⁺ neurons in the PoA inhibit, directly or indirectly, downstream Crh⁺ neurons, preventing overactivation of the HPI axis (Figure 7G). This inhibition is likely mediated by GABAergic transmission. The neuropeptide Galn instead mediates an additional control system regulating activity of Galn⁺ neurons, by reducing their activation through an autocrine mechanism. This dual control system likely regulates a balance of inhibition over Crh⁺ neurons, which allows fine tuning neuroendocrine and behavioral responses to stressful situations.

Acknowledgments

We would like to thank Anne Banerjee, Bastiaan Pierik, Steffen Tornow, and the staff of the Zebrafish Facility and the Advanced Light Microscopy Technology Platform at the Max Delbrück Center for Molecular Medicine for technical support. We are also thankful to Margerita Zaupa for critical input on data analysis and providing reagents, Onur Apaydin for data analysis, and Prof. Pertti Panula for providing us with the plasmid for synthesizing the *galn in situ* probe. Prof. Herwig Baier kindly provided us with zebrafish lines. This work was supported by the Helmholtz Association of German Research Centers, and by a grant from the German Research Foundation (Deutsche Forschungsgemeinschaft, project ID: FI 2339/3-1).

Author Contributions

A.F. conceived and designed experiments, provided supervision, administered the project, and performed data analyses. S.S. and M.d.M. provided supervision and designed experiments. L.C. conceived, designed, and performed experiments, and analyzed data. M.d.M. and M.B.

performed experiments and data analyses. A.F. and L.C. wrote the manuscript. All authors commented on the manuscript.

Declaration of interests

The authors declare no competing interests.

Figure legends

Figure 1. Galn⁺ neurons are activated by stressors (see also Figure S1, S2, S3). **A.** Schematic illustration depicting location of Galn⁺ neurons in the zebrafish brain (left), and maximum projection of a confocal stack showing localization of Galn⁺ neurons in a 5 dpf *galn:Gal4; UAS:NTR-mCherry* larva (right). Neurons are color-coded according to their depth. A and P indicate anterior and posterior directions, respectively. Scale bar = 25 μ m. **B.** Confocal images of 5 dpf *galn:Gal4; UAS:EGFP* fish immunostained with antibodies against GFP, pERK, and tERK. Scale bar = 25 μ m. **C – F.** Graphs depicting cumulative fractions of pERK/tERK values in Galn⁺ neurons in 5 dpf *galn:Gal4; UAS:EGFP* larvae localized in the PoA (C, E) or in the pHyp (D, F), after exposure to the hypertonic solution (C, D) or intense blue light (E, F). In (C) $n_{\text{control}} = 117$ neurons from 7 larvae, $n_{\text{NaCl}} = 132$ neurons from 7 larvae. In (D) $n_{\text{control}} = 204$ neurons from 7 larvae, $n_{\text{NaCl}} = 239$ neurons from 7 larvae. In (E) $n_{\text{control}} = 218$ neurons from 10 larvae, $n_{\text{blue light}} = 172$ neurons from 9 larvae. In (F) $n_{\text{control}} = 219$ neurons from 7 larvae, $n_{\text{blue light}} = 146$ neurons from 6 larvae. * $p < 0.05$, *** $p < 0.001$, n.s. = not significant, two-sample Kolmogorov-Smirnov test.

Figure 2. Galn⁺ neurons in the PoA are a heterogeneous population displaying diverse responses to a stressor (see also Figure S4, S5). **A.** Image showing Galn⁺/GCaMP6s⁺ neurons in the PoA of a 5 dpf *galn:Gal4; UAS:GCaMP6s* larva. Scale bar = 25 μ m. **B.** $\Delta F/F_0$ traces representative of the four response types of Galn⁺ neurons. The colored rectangle indicates presence of the 100 mM NaCl solution. **C.** Pie chart showing percentages of

response types in Galn⁺ neurons in the PoA. **D, E.** Bar graphs depicting average frequency (D) and amplitude (E) of calcium transients in Galn⁺ neurons in the PoA before (baseline) and after (NaCl) exposure to the hypertonic solution. In (C – E) data were obtained from 24 (increased activity group), 8 (decreased activity group), and 3 (non responsive and inactive groups) larvae. Color coding as in (C). Data in (D) and (E) are shown as mean ± SEM. n = number of neurons. *** p < 0.001, n.s. = not significant, two-tailed t-test. Statistical tests were not performed in (D) because frequency was already used as a parameter for classification of neuronal types. **F, G.** Scatter plots showing spatial localization of Galn⁺ neurons in the PoA, displayed as top (F) and lateral (G) view. Colors indicate the different types of stressor-response profile, as shown in (C). Each dot represents a Galn⁺ neuron. Data were obtained from 20 larvae. AC = anterior commissure. **H.** Plot depicting the relation between correlation of activity (Pearson correlation coefficient) and physical distance between Galn⁺ neurons in the PoA of four 5 dpf *galn:Gal4; UAS:GCaMP6s* larvae. Colors indicate the larvae from which Galn⁺ neurons were analyzed.

Figure 3. Ablation of Galn⁺ neurons causes increased stress-related behavioral responses. **A.** Scheme of the timeline of application of the hypertonic solution (NaCl), and formula for calculating motility ratio. **B.** Graph depicting average spontaneous locomotion of 5 dpf larvae with (control) or without (ablated) Galn⁺ neurons. **C, D.** Graphs showing average motility ratios during two time windows after application of the NaCl solution, 0 min to 10 min (C) or 10 min to 20 min (D) after the end of the baseline period. **E.** Bar graph displaying average whole-body cortisol amounts in 5 dpf larvae either with (control) or without (ablated) Galn⁺ neurons after administration of the hypertonic solution for 10 minutes. **F.** Graph depicting average startle probability of 5 dpf Galn⁺-neurons-ablated or control larvae. **G.** Confocal images showing two Galn⁺ neurons before and after two-photon-laser-mediated cell ablation. Only the targeted cell (arrow) was efficiently ablated, leaving the other one intact. Scale bar = 10 μm. **H.** Graph depicting average spontaneous locomotion in 5 dpf *galn:Gal4; UAS:EGFP* larvae in which Galn⁺ neurons in the PoA were laser-ablated (PoA ablation), or in control

unablated fish. **I, J.** Graphs showing average motility ratios of control and PoA ablated larvae during two time windows after application of the hypertonic solution, 0 min to 10 min (I) or 10 min to 20 min (J) after the end of the baseline period. Data are shown as mean \pm SEM. n = number of larvae, except in (E) where it indicates number of biological replicates obtained by pooling 20 – 25 larvae each. * p < 0.05, ** p < 0.01, n.s. = not significant, two-tailed t-test.

Figure 4. Lack of Galn decreases stress-related behavioral responses, while overexpression of galn increases them. **A.** Sequences of part of the wild type and mutated *galn* gene containing a deletion of 11 base pair (bp) in the exon 3. **B.** Images showing immunofluorescence staining of the neuropeptide Galn in 5 dpf *galn*^{+/+} and *galn*^{md76/md76} larvae. No Galn was detected in homozygous mutant larvae. Scale bar = 25 μ m. **C – E.** Graphs depicting average spontaneous locomotion (C), and average motility ratios during two time windows after application of the hypertonic solution, 0 min to 10 min (D) or 10 min to 20 min (E) after the end of the baseline period, of 5 dpf *galn*^{+/+}, *galn*^{+/md76}, and *galn*^{md76/md76} larvae. **F.** Scheme depicting the DNA construct used to overexpress *galn* in Galn⁺ neurons, by injecting it in *galn:Gal4* embryos at one-cell stage. **G.** Maximum projection of a confocal stack showing Galn⁺/tdTomato-CAAX⁺ neurons in 5 dpf *galn:Gal4* larvae previously injected with the *UAS:galn-T2A-tdTomato-CAAX* construct. Scale bar = 40 μ m. **H – J.** Bar graphs depicting average motility ratios during two time windows after application of the hypertonic solution, 0 min to 10 min (H) or 10 min to 20 min (I) after the end of the baseline period, and average spontaneous locomotion in the absence of the stressor (J) of 5 dpf *galn:Gal4* larvae injected with the *UAS:galn-T2A-tdTomato-CAAX* construct. *galn:Gal4*. Wild-type clutchmates lacking the *galn:Gal4* transgene, and injected with the *UAS:galn-T2A-tdTomato-CAAX* cassette, were used as controls in the data sets shown in (H – J). Data are shown as mean \pm SEM. n = number of larvae. * p < 0.05, ** p < 0.01, n.s. = not significant, two-tailed t-test.

Figure 5. Galn⁺ neurons in the PoA are GABAergic and express genes coding for Galn receptors. **A.** Images showing localization of *gad2* transcript, detected with fluorescence *in*

situ HCR, in Galn⁺ neurons in the PoA of a 5 dpf *galn:Gal4; UAS:EGFP* larva. Scale bar = 5 μm. **B.** Graph depicting percentages of Galn⁺ neurons expressing *gad2* in the PoA. **C.** Fluorescence *in situ* HCR for *galnR1a* and *galnR1b* transcripts in a 5 dpf *galn:Gal4; UAS:EGFP* larva. The arrow and arrowheads indicate localization of *galnR1a* and *galnR1b* mRNAs in Galn⁺ neuron, respectively. Scale bar = 5 μm. **D.** Percentages of Galn⁺ neurons expressing *galnR1a* or *galnR1b* in the PoA. **E.** Fluorescence *in situ* HCR for *galnR2a* and *galnR2b*. The arrow indicates presence of *galnR2b* mRNA in a Galn⁺ neuron. Scale bar = 5 μm. **F.** Percentages of Galn⁺ neurons expressing *galnR2a* or *galnR2b* in the PoA. No Galn⁺ neurons expressing *galnR2a* were observed. Data are shown as mean ± SEM. n indicates number of fish.

Figure 6. Galn reduces activation of Galn⁺ neurons (see also Figure S6). **A.** Scheme summarizing the hypothesized modulatory action of Galn⁺ neurons and Galn on stress-promoting neurons. (Left) Galn⁺ neurons send GABAergic inhibitory inputs to a population of stress-promoting neurons. Stressful stimuli lead to the release of Galn from Galn⁺ neurons, which binds to autoreceptors on Galn⁺ cells, reducing their activity. (Right) In *galn^{md76/md76}* larvae, Galn is absent and cannot negatively modulate the activity of Galn⁺ cells. Consequently, Galn⁺ neurons release more GABA onto the downstream neuronal populations, ultimately resulting in decreased stress responses. **B.** Pie charts showing percentages of response types in Galn⁺ neurons in the PoA of 5 dpf *galn:Gal4; UAS:GCaMP6s; galn^{+/+}* and *galn:Gal4; UAS:GCaMP6s; galn^{md76/md76}* fish. Percentages of the four different types of responses were not substantially different between *galn^{+/+}* and *galn^{md76/md76}* larvae. **C, D.** Graphs showing frequency of calcium events in the “increased activity” (C) and “decreased activity” (D) types of Galn⁺ neurons in 5 dpf *galn:Gal4; UAS:GCaMP6s; galn^{+/+}* and *galn:Gal4; UAS:GCaMP6s; galn^{md76/md76}* fish before (baseline) and after (NaCl) application of the hypertonic solution. **E.** Pie charts depicting percentages of the four types of Galn⁺ neurons in the PoA of 5 dpf *galn:Gal4; UAS:GCaMP6s* larvae injected at one-cell-stage embryo either with the control *UAS:tdTomato-CAAX* or the *UAS:galn-T2A-tdTomato-CAAX* constructs. **F, G.**

Graphs showing frequency of calcium events in the “increased activity” (F) and “decreased activity” (G) types of Galn⁺ neurons in 5 dpf *galn:Gal4; UAS:GCaMP6s* fish, injected with the *UAS:tdTomato-CAAX* or the *UAS:galn-T2A-tdTomato-CAAX* plasmid, before (baseline) and after (NaCl) application of the hypertonic solution. Data in the bar graphs are shown as mean \pm SEM. In (C) $n_{galn^{+/+}} = 36$ neurons from 19 larvae, $n_{galn^{md76/md76}} = 36$ neurons from 22 larvae. In (D) $n_{galn^{+/+}} = 7$ neurons from 6 larvae, $n_{galn^{md76/md76}} = 9$ neurons from 5 larvae. In (F) $n_{UAS:tdTomato-CAAX} = 33$ neurons from 18 larvae, $n_{UAS:galn-T2A-tdTomato-CAAX} = 28$ neurons from 17 larvae. In (G) $n_{UAS:tdTomato-CAAX} = 5$ neurons from 3 larvae, $n_{UAS:galn-T2A-tdTomato-CAAX} = 5$ neurons from 5 larvae. * $p < 0.05$, ** $p < 0.001$, n.s. = not significant, two-tailed t-test.

Figure 7. Galn⁺ neurons negatively modulate activity of Crh⁺ neurons in the PoA (see also Figure S7). **A.** (Top) Graphs depicting mean activity (z score) of “increased activity” type Galn⁺ neurons (left) or Crh⁺ neurons (right) in the PoA of four 5 dpf *galn:Gal4; UAS:NTR-mCherry; elavl3:H2B-GCaMP6s* larvae, before and after exposure to 100 mM NaCl. Crh⁺ neurons were identified *post mortem* using fluorescence *in situ* HCR, and subdivided in “increased activity” or “decreased activity” types following the same method used to classify Galn⁺ neurons (see Star Methods). (Bottom) Raster plots displaying activity (z scores) of each Galn⁺ and Crh⁺ neuron used to generate the mean z score traces. Crh⁺ neurons of the “increased activity” and “decreased activity” types are labeled with red and teal numbers, respectively. To enhance neuronal activity visualization, the scale of the color bar was adjusted by narrowing the range to 0–1. **B.** Graph showing cross-correlation between activity of “increased activity” type Galn⁺ cells and Crh⁺ neurons after exposure to 100 mM NaCl. The “decreased activity” type Crh⁺ neurons initially displayed a positive cross-correlation with Galn⁺ neurons, which then turned to negative values after Galn⁺ neurons reached their peak of average activity. **C.** Confocal images showing *crhb* localization and pERK and tERK immunostainings in the PoA of a 5 dpf wild type larva. Scale bar = 25 μ m. **D.** Graph depicting cumulative fractions of pERK/tERK values in Crh⁺ neurons in the PoA of 5 dpf control non-ablated larvae (treated with nifurpirinol) following two minutes exposure to 100 mM NaCl or

control saline solution. $n_{\text{saline}} = 70$ neurons from 11 larvae, $n_{\text{NaCl}} = 60$ neurons from 11 larvae. **E, F.** Graphs showing cumulative fractions of pERK/tERK values in Crh⁺ neurons in the PoA of 5 dpf larvae lacking Galn⁺ neurons (ablated) and non-ablated control siblings treated with 100mM NaCl (E) or saline solution (F) for two minutes. In (E) $n_{\text{control}} = 60$ neurons from 11 larvae, $n_{\text{ablated}} = 57$ neurons from 12 larvae. In (F) $n_{\text{control}} = 70$ neurons from 11 larvae, $n_{\text{ablated}} = 65$ neurons from 14 larvae. *** $p < 0.001$, two-sample Kolmogorov-Smirnov test. **G.** Model summarizing our findings. Galn⁺ neurons inhibit downstream stress-promoting Crh⁺ neurons, possibly via either direct or indirect GABAergic connections, and consequently prevent activation of the HPI axis in basal conditions, and its overactivation when stressors are present. The neuropeptide Galn fine tunes activity of Galn⁺ neurons through an autocrine inhibitory mechanism, thus regulating the intensity of inhibition on Crh⁺ neurons.

STAR+METHODS

KEY RESOURCES TABLE

REAGENT or RESOURCE	SOURCE	IDENTIFIER
Antibodies		
polyclonal chick Anti-GFP	Thermo Fisher	Cat# A10262; RRID: AB_2534023
monoclonal mouse Anti-p44/42 MAP Kinase	Cell Signaling	Cat# 4696; RRID: AB_390780
monoclonal rabbit Anti-p44/42 MAP Kinase (Thr202/Tyr204)	Cell Signaling	Cat#4370; RRID: AB_2315112
monoclonal rat anti-mCherry	Thermo Fisher	Cat# M11217; RRID: AB_2536611
polyclonal rabbit anti-Galanin	Millipore	Cat# AB5909, RRID:AB_21085 17
Alexa Fluor 405 Anti-rabbit	Thermo Fisher	Cat# A-31556, RRID:AB_22160 5
Alexa Fluor 488 Anti-mouse	Cell Signaling	Cat# 4408; RRID: AB_10694704
Alexa Fluor 488 Anti-chicken	Thermo Fisher	Cat# A11039; RRID: AB_142924

Alexa Fluor 647 Anti-mouse	Cell Signaling	Cat# 4410S; RRID: AB_1904023
Alexa Fluor 647 Anti-rabbit	Thermo Fisher	Cat# A31573; RRID: AB_2536183
Alexa Fluor 555 Anti-rabbit	Cell Signaling	Cat# 4413; RRID: AB_10694110
Alexa Fluor 555 Anti-rat	Cell Signaling	Cat# 4417; RRID: AB_10696896
Anti-DIG-AP	Roche	Cat# 11093274910; RRID: AB_514497
Chemicals, peptides, and recombinant proteins		
Trypsin-EDTA	Sigma	Cat# T4049
Nifurpirinol	Sigma	Cat# 32439
Agarose, Low Melting Point	Roboklon	E0303-50
Tricaine (3-amino benzoic acidethylester)	PHARMAQ	N/A
Dimethyl sulfoxide (DMSO)	Th. Geyer	Cat# 23419.3
Pancuronium bromide	Sigma	Cat# P1918
Triton X 100	Roth	Cat# 3051.3
Tween 20	Roth	Cat# 9127.2
Bovine Serum Albumin	Serva	Cat# 11943.02
Paraformaldehyde (PFA)	Sigma	Cat# P6148
Goat serum	Sigma	Cat# G6767
DIG-labeling mix	Roche	Cat# 11277065910
NBT/BCIP	Sigma	Cat# B5655
Proteinase K	Sigma	Cat# 3115879001
Critical commercial assays		
Cortisol ELISA Kit	Biomol	500360-96
HCRv3 reagents	Molecular Instruments	https://www.molecularinstruments.com/
Experimental models: Organisms/strains		
Zebrafish: <i>TgBAC[galn:GAL4-VP16,myl7:mCherry]_{mpn213}</i>	28	ZFIN: ZDB-ALT-170908-13
Zebrafish: <i>Tg[5xUAS:EGFP]^{nkuasgfp1a}</i>	57	ZFIN: ZDB-ALT-080528-1
Zebrafish: <i>Tg[UAS-E1b:NTR-mCherry]^{c264}</i>	58	ZFIN: ZDB-ALT-070316-1
Zebrafish: <i>Tg[14xUAS:GCaMP6s]^{mpn101}</i>	59	ZFIN: ZDB-ALT-140811-3
Zebrafish: <i>Tg[elav13:H2B-GCaMP6s]^{jj5}</i>	60	ZFIN: ZDB-ALT-141023-2
Zebrafish: <i>galn^{md76}</i>	This paper	N/A
Oligonucleotides		
SgRNA targeting sequence: CGGACTCACGAGGACCGAGG	46	N/A

Galn_F: ACATTTTGTGTAAAACAGGCAAAAG	Eurofins Genomics	N/A
Galn_R: GTAGACCTGAGAGCAGCATGA	Eurofins Genomics	N/A
Galn_Kozak_F: CGGAATTCGCCGCCACATGCACAGGTGTGTC	Eurofins Genomics	N/A
Galn_Srfl_R: GGCCCGGGCGTCGCTGAGGCTCCT	Eurofins Genomics	N/A
Recombinant DNA		
Plasmid: <i>UAS:galn-T2A-tdTomato-CAAX</i>	This paper	N/A
Plasmid: <i>UAS:tdTomato-CAAX</i>	This paper	N/A
Software and algorithms		
Fiji/ImageJ	NIH	https://fiji.sc/
Prism version 7	GraphPad Software	https://www.graphpad.com/scientific-software/prism/
EthoVision XT version 8.5	Noldus	https://www.noldus.com/ethovision-xt
MATLAB	The MathWorks	https://www.mathworks.com/products/matlab.html
Python	Python Software Foundation	https://www.python.org/
ANTs (Anatomical Normalization Toolkits)	⁶⁶	http://stnava.github.io/ANTs/
ZEN software	Zeiss	N/A
Python code for startle behavior	This paper	DOI: 10.5281/zenodo.5897926
Other		
Camera	XIMEA	Cat# MQ003MG-CM
Power Meter Photodiode Sensor	Thorlabs	Cat# S170C

RESOURCE AVAILABILITY

Lead contact

Further information and requests for resources and reagents should be directed to and will be fulfilled by the lead contact, Alessandro Filosa (Alessandro.Filosa@mdc-berlin.de).

Materials availability

Plasmids and zebrafish lines generated in this study are available upon request.

Data and code availability

- All data reported in this paper will be shared by the lead contact upon request.
- All original code has been deposited at Zenodo and is publicly available as of the date of publication. DOIs are listed in the key resources table.
- Any additional information required to reanalyze the data reported in this paper is available from the lead contact upon request.

EXPERIMENTAL MODEL AND SUBJECT DETAILS

Zebrafish lines and maintenance

All zebrafish experiments were performed on larvae not older than 5 dpf. Zebrafish were kept under standard conditions at 28.5°C on a 14 hr/10 hr light/dark cycle. Embryos and larvae were raised in Danieau's medium (58 mM NaCl, 0.7 mM KCl, 0.4 mM MgSO₄, 0.6 mM Ca(NO₃), 2.5 mM HEPES, pH adjusted to 7). All animal procedures were conducted in accordance with institutional (Max Delbrück Center for Molecular Medicine), State (LAGeSo Berlin), and German ethical and animal welfare guidelines and regulations. Sex of zebrafish cannot be determined at the developmental stages considered in this study. Animals were randomly assigned to experimental groups.

The following previously established transgenic lines were used in this study: *Tg[galn:Gal4-VP16]^{mpn213,28}*, *Tg[5xUAS:EGFP]^{nkuasgfp1a,57}*, *Tg[UAS-E1b:NTR-mCherry]^{p264,58}*, *Tg[14xUAS:GCaMP6s]^{mpn101,59}*, *Tg[elavl3:H2B-GCaMP6s]^{jf5,60}*.

The *galn^{md76}* mutant line was generated using a CRISPR/Cas9 mutagenesis strategy.⁴⁶ Cas9 protein (generated in-house) at a final concentration of 0.6 µg/µl was co-injected with a sgRNA (400 ng/µl) with the targeting sequence 5'-CGGACTCACGAGGACCGAGG-3'. The mutant allele contains an 11 base-pairs insertion in exon 3 leading to a frameshift mutation and premature stop codon. Larvae for the experiments were obtained by incrossing *galn^{+/md76}* heterozygous mutants. Genotyping was carried out by PCR using the primers 5'-ACATTTTGTGTAAAACAGGCAAAAG-3' and 5'-GTAGACCTGAGAGCAGCATGA-3' which leads to amplification of a 177 bp DNA fragment. After BsaJI (New England Biolabs, Cat# R0536) digestion, the wild type allele produces two bands of 34 bp and 104 bp, whereas the

restriction enzyme site is missing in the *galn*^{md76} mutant allele, leaving the 177 bp DNA fragment intact.

Unless otherwise stated, experiments were performed with AB/TL mixed strain zebrafish.

METHOD DETAILS

Generation of plasmids

To generate the *UAS:galn-T2A-tdTomato-CAAX* plasmid, the *galn* coding sequence was amplified by PCR from a 5 dpf zebrafish cDNA library using the primers Galn_Kozak_F CGGAATTCGCCGCCACATGCACAGGTGTGTC and Galn_Srf1_R GGCCCGGGCGTCGCTGAGGCTCCT. The amplified *galn* coding sequence was cloned in a pTol2 plasmid, downstream of 14 *UAS* sequences using Ecor1 and Not1 restriction sites. The *T2A-tdTomato-CAAX* cassette was amplified by PCR and then cloned downstream of the *galn* sequence using a Srf1 restriction site. To generate the *UAS:tdTomato-CAAX* plasmid the *tdTomato-CAAX* cassette was cloned downstream of the *UAS* sequences of the *pTol2* plasmid.

Injection of plasmids in zebrafish embryos

For calcium imaging experiments, *galn:Gal4; UAS:GCaMP6s* zebrafish were injected at one-cell stage with the *UAS:galn-T2A-tdTomato-CAAX* or *UAS:tdTomato-CAAX* constructs and larvae were live imaged at 5 dpf. For the behavioral experiments, the *UAS:galn-T2A-tdTomato-CAAX* construct was injected at one-cell stage in *galn:Gal4* embryos. After performing behavioral experiments, the expression of the construct was verified using a confocal microscope, and larvae displaying expression of the *galn-T2A-tdTomato-CAAX* transgene were allocated in the experimental group, while non-expressing fish were used as controls.

Immunohistochemistry and *in situ* hybridization

Larvae were anesthetized with tricaine and fixed with 4% paraformaldehyde (PFA) in PBS with 0.3% Triton (PBT) overnight at 4°C. Immunohistochemistry was performed based on a

previously described protocol.⁶¹ Larvae were washed with PBT and incubated in 150 mM Tris-HCl (pH 9) for 5 min at room temperature followed by 15 min at 70°C. Larvae were washed in PBT before they were incubated in Trypsin EDTA (Sigma-Aldrich #T4299, diluted 1:50 in PBT) for 40 minutes on ice. After PBT washes, larvae were blocked in 5% goat serum, 1% bovine serum albumin, and 1% DMSO in PBT for 1 hour at room temperature. Primary antibodies (1:500 dilution) were added in blocking solution (5% goat serum, 1% bovine serum albumin, and 1% DMSO in PBT) for 96 hours at 4°C. Larvae were washed in PBT, and secondary antibodies (1:300 dilution) were added for 48 hours at 4°C. Primary antibodies against the following antigens were used: total ERK (Cell Signaling, Cat# 4696), phosphorylated ERK (Cell Signaling, Cat# 4370), GFP (Invitrogen, Cat# A10262), mCherry (ThermoFisher, Cat# M11217), Galanin (Sigma, Cat# AB5909). The following Alexa Fluor secondary antibodies were used: AF488- α -chicken (ThermoFisher, Cat# A11039), AF555- α -rabbit (Cell Signaling, Cat# 4413), AF555- α -rat (Cell Signaling, Cat# 4417), AF647- α -mouse (Cell Signaling, Cat# 4410) and AF647- α -rabbit (ThermoFisher, Cat# A31573).

Colorimetric *in situ* hybridization was performed as described previously⁶² using a *galn* antisense probe.⁶³ In short, larvae were digested with proteinase K (final solution 10 μ g/mL) for 40 minutes at room temperature and post-fixed with 4% PFA. Samples were blocked in hybridization buffer (50% formamide, 2x SSC, 50 μ g/ μ L heparin, 5 mg/mL torula-RNA, 0.1% tween20, 5% dextran sulfate) and incubated overnight at 70°C with the digoxigenin labeled probe against *galn*. Probes were washed with SCC and then blocked with BSA 2 mg/mL and 2% Goat serum in PBS with 0.1% Tween20 (PBST) for 2 hours at room temperature. Anti-DIG-AP antibody (Roche, Cat #11093274910, 1:5000 dilution) was added in blocking solution overnight at 4°C. PBST-washed larvae were incubated in Nitro blue tetrazolium chloride (NBT)/5-Brom-4-chlor-3-indoxylphosphat (BCIP) (Sigma, Cat # B5655) solution, and the enzyme reaction was stopped with several washes in PBST once the signal was observed.

The third-generation fluorescence *in situ* HCR v.3.0³⁹ was used to detect *crhb*, *gad2*, *galnR1a*, *galnR1b*, *galnR2a*, and *galnR2b* transcripts. The *in situ* probes and the dye-conjugated hairpins were purchased from Molecular Instruments Inc., and the HCR v.3.0 was performed

according to manufacturer's instructions. Briefly, larvae were permeabilized using proteinase K (final solution 30 $\mu\text{g}/\text{mL}$) for 45 minutes, post-fixed in 4% PFA and incubated overnight at 37°C in probe hybridization buffer containing 1 pmol of each probe. Probes were washed at 37°C with wash buffer prior to overnight incubation in amplification buffer containing 30 pmol of each fluorescently labelled hairpin. Following HCR, larvae were washed with PBST, and primary and secondary antibodies were added in blocking solution as described earlier. PBST-washed larvae were then embedded in 1.5% low-melting-point agarose for confocal imaging.

Confocal microscopy

Images were acquired using a Zeiss LSM880 confocal microscope equipped with a 20X objective (W Plan- Apochromat 20x/1.0 DIC VIS-IR, Zeiss). For the pERK/tERK experiments all larvae were imaged using constant acquisition settings. GFP-positive cells in *galn:Gal4; UAS:EGFP* larvae and Crh⁺ cells labeled with the HCR probe for *crhb* were manually selected to measure the fluorescent intensities of pERK and tERK immunostainings using ImageJ. Galn⁺ cells in the PoA colocalizing with *gad2* or *galnR* transcripts were counted in ImageJ.

Calcium imaging

Larvae used for calcium imaging experiments were *mitfa*^{-/-} mutants lacking skin melanophores.⁶⁴ Larvae were embedded in 1% low-melting-point agarose containing 0.3 mg/mL pancuronium bromide (Sigma, Cat# P1918) to immobilize the fish. Imaging was performed using a Zeiss LSM880 NLO confocal microscopy system equipped with 20X water-immersion objective (W Plan- Apochromat 20X/1.0 DIC VIS-IR, Zeiss). Time series were recorded at a resolution of 256 × 256 pixels and a frame rate of 5 frames per second (fps). Embedded larvae were acclimatized at room temperature in 2.5 mL of Danieau's solution for at least 20 minutes before imaging. Control or stress stimuli were applied after 120 seconds of baseline recording by adding 50 μl of Danieau's solution (control experiment) or 50 μl of a 5 M NaCl solution (hyperosmotic stressor) to the Petri dish containing the larva (obtaining a final 100 mM concentration). For the experiments in which two stress stimuli were applied

consecutively, the Petri dish was rapidly washed from the hypertonic solution used for the first stimulation and replaced with 2.5 mL of Danieau's solution. The larvae were then left at room temperature for 30 minutes before the second stimulus consisting of 50 μ l of a 5 M NaCl solution was applied. Image time series were x-y motion-corrected using a modified version of the NoRMCorre algorithm.⁶⁵ To identify calcium transients the event detection algorithm MLspike⁶⁶ was used. GCaMP6s fluorescence was measured using ImageJ by manually selecting regions of interest. $\Delta F/F_0$ was calculated as $(F - F_0)/F_0$, where F_0 and F are the average baseline fluorescence intensity and fluorescence intensity at different time points, respectively. The number of calcium events during the baseline recording (120 seconds) was compared with the total numbers of calcium events during the 120 seconds after administration of NaCl to manually categorize the neurons according to their activity. Neurons were classified as "increased activity" if the number of Ca^{2+} events increased at least by 5% after NaCl exposure, compared to baseline, "decreased activity" when the number of events was reduced at least by 5%, or "invariant" when the change of frequency of Ca^{2+} events was less than 5%. Neurons were defined as inactive when no Ca^{2+} events were detected during the imaging. Data were analyzed using ImageJ, MATLAB and Microsoft Excel.

To map the position of the $Galn^+$ cells in the PoA, *galn:Gal4; UAS:GCaMP6s* larvae were fixed with 4% PFA in PBT after calcium imaging experiments and immunostained for GFP and tERK. To obtain the anatomical coordinates of the neurons, we measured in each larva in ImageJ the distances of the neurons from the posterior edge of the anterior commissure (for antero-posterior positioning), from the midline (for left-right positioning), and from the dorsal edge of the anterior commissure (for dorsal-ventral positioning).

In the experiments aiming at characterizing the responses of $Galn^+$ and Crh^+ cells, a multiphoton system (Thorlabs, Bergamo I series) equipped with an Electro-Tunable Lens (ETL, Optotune EL-10-30-C-NIR-LD-MV, O) for multiplane imaging⁶⁷ was used for recordings in 5 dpf *galn:Gal4; UAS:NTR-mCherry; elav:H2BGCaMP6s* larvae. Following the same protocol described above, we sampled a volume (400 x 200 x 180 μ m³), which included the PoA, with 30 planes at one volume per second with 1024 x 512 pixels per plane and a relative z-spacing

of circa 6 μm . For each fish, at the end of the functional recordings, reference high-resolution z-stacks of the whole brain were acquired for the anatomical co-registration and identification of the Crh^+ neurons. Afterward, larvae were anesthetized with tricaine and fixed with 4% PFA in PBS overnight at 4°C. The fluorescence *in situ* HCR v.3.0 method was then used, as described above, to detect *crhb* mRNA and identify Crh^+ neurons.

We implemented an anatomical registration pipeline based on ANTs (Anatomical Normalization Toolkits)⁶⁸ for identifying Crh^+ neurons, revealed by fluorescence *in situ* HCR, in the temporal series acquired from the same fish. Briefly, we registered the GCaMP channel of the z-stack acquired from each live fish to a live template of the brain atlas and applied the transformation already refined in⁶⁹ to obtain the anatomical space corresponding to the GCaMP channel of the fixed reference brain available in the atlas. To this very same reference channel, similarly, the GCaMP channel of the fixed brain, with the *crhb* fluorescence *in situ* HCR signals, was registered for each fish and the corresponding transformation applied to the channels with labelled Crh^+ and Galn^+ neurons. The respective transformations were then applied to the x, y, z coordinates of the Crh^+ neurons from the fluorescence *in situ* HCR and the GCaMP neurons from the functional recordings.

To measure the registration accuracy, we first inspected manually the registered stacks for successful alignment. Next, we identified various Galn^+ neurons in the reference channel of the standard brain that were also present in the registered stacks and saved their x, y, z coordinates in Fiji/ImageJ. The calculated distances varied between 2 μm and 9 μm with a median of 5.84 μm .

For characterizing the dynamics of the different Crh^+ neuronal sub-populations with respect to the Galn^+ neurons, we computed the cross correlation on segments of the mean time series corresponding to the 60 seconds following the NaCl perfusion using the python signal processing library Scipy.Signal (<https://docs.scipy.org/doc/scipy/reference/signal.html>).

Nitroreductase-mediated cell ablations

galn:Gal4; UAS:NTR-mCherry larvae and control fish (lacking NTR expression) were both treated with 2.5 μ M nifurpirinol (Sigma, Cat# 32439) plus 0.5% DMSO in Danieau's solution from 3 dpf until 4 dpf, and with 5 μ M nifurpirinol plus 0.5% DMSO from 4 dpf till 5 dpf. At 5 dpf the drug was removed and the stress treatments or the behavioral experiments were performed after 5 hours. Fish were kept in the dark during nifurpirinol treatment to prevent inactivation of the drug. Efficiency of ablation was verified using a fluorescent stereomicroscope or a confocal microscope after performing behavioral experiments or prior to exposure to hyperosmotic stress.

Laser-mediated cell ablations

To perform two-photon-laser-mediated neuronal ablations, 4 dpf larvae were anesthetized with 0.016% tricaine and embedded in 1% low-melting-point agarose. A TiSa two-photon laser, set at 880 nm was used for ablating Galn⁺ neurons in *galn:Gal4; UAS:EGFP* larvae. Each neuron of interest was laser irradiated for approximately 50 ms to ablate the cells. Approximately 90% of the EGFP⁺ neurons in the PoA were ablated in each fish. To exclude the possibility that the laser pulse could damage cells surrounding the targeted neurons, we performed the procedure, using the same laser pulse duration and power, on 5 dpf *galn:Gal4; UAS:NTR-mCherry; elavl3:H2B-GCaMP6s* larvae. Inspection of the selected brain region the day after the procedure revealed that only the targeted Galn⁺ neurons, and no other surrounding cells, were damaged. We performed behavioral tests after approximately 24 hours, to allow larvae to recover from the potential stress caused by the ablation procedure. After behavioral experiments, the treated larvae were re-imaged using a confocal microscope to confirm efficient ablation of neurons.

Exposure to hyperosmotic stress

Groups of approximately 20 larvae were placed in 60 mm Petri dishes with 15 mL of Danieau's solution and left at room temperature for at least one hour before starting experiments. To induce hyperosmotic stress 15 mL of a 200 mM NaCl solution was added to each experimental

Petri dish (to obtain a final concentration of 100 mM), while 15 mL of Danieau's solution was added to control groups. Larvae were incubated for two or ten minutes in the solution before being anesthetized with tricaine and rapidly fixed with 4% PFA in PBT for immunostaining, with 4% PFA in PBS for *in situ* hybridization, or frozen at -80°C for cortisol measurements.

Blue-light-induced stress

Groups of approximately 20 larvae were placed in 60 mm Petri dishes with 15 mL of Danieau's solution and dark-adapted for 40 minutes prior to experiment. Experimental groups were exposed for five minutes to a one second pulse of flashing blue light (470 nm) delivered at 30Hz (Figure S2). Light power, 2.8 mW cm^{-2} , was measured using a Power Meter Photodiode Sensor (Thorlabs, Cat# S170C). Light was delivered through a custom-built array of LEDs positioned at a fixed distance below the Petri dish to allow homogeneous illumination. Control and experimental groups were then anesthetized and rapidly fixed with 4% PFA in PBT for immunostaining.

Behavioral assays

Experiments were conducted in a custom-made behavioral setup placed on a vibration isolation table at $28 \pm 0.5^\circ\text{C}$. For the locomotion assays larvae were imaged at 40 fps using a high-speed camera (XIMEA GmbH, Cat# MQ003MG-CM) positioned above a swimming chamber. In the startle-response experiments larvae were imaged at 500 fps.

In all experiments, multiwell plates containing the larvae were placed in the behavioral setup at least 10 minutes before starting video acquisition. Control and experimental animals were handled in the same fashion and recorded simultaneously.

For locomotion assays, prior to the experiment, larvae were placed in a multiwell plate with each well holding 100 μL of Danieau's solution. Larvae were imaged for an initial period of 10 minutes (baseline locomotion). After addition of 100 μL of 200 mM NaCl (final concentration 100 mM) to induce hyperosmotic stress, fish were imaged for 20 minutes. EthoVision XT

(Noldus Information Technology, version 8.5) was used to measure the distance moved by each larva.

After behavioral experiments, *galn:Gal4* larvae injected with the *UAS:galn-T2A-tdTomato-CAAX* were imaged using a confocal microscope to confirm expression of the construct.

To elicit acoustic startle responses, sound stimuli of 3-ms duration and 13-dB intensity were generated with a custom Python code and delivered by two speakers positioned at the sides of the multiwell containing the larvae. A baseline of one second and an interval of one second after stimulus onset were recorded with a high-speed camera at 500 fps. Intervals between stimuli lasted 120 seconds. Behavioral responses were classified as startle responses if larvae displayed a rapid movement of the body initiated no later than 50 ms from the end of the stimulus. Responses were recorded as a binary variable (1 for response and 0 for no response) through five repetition to calculate the startle probability.

Cortisol measurements

Following osmotic stress, zebrafish larvae were pooled in groups of approximately 20 – 25 individuals, anesthetized with tricaine and frozen at -80°C. Samples were lysated with a tissue homogenizer and cortisol was extracted following a previously described protocol.⁷⁰ Cortisol amounts were then measured using an enzyme immunoassay detection kit (Caymanchem, Cat# 500360-96) according to the manufacturer's instructions.

QUANTIFICATION AND STATISTICAL ANALYSIS

Statistical significance was determined using two-tailed Student's t tests in Microsoft Excel and GraphPad Prism (GraphPad, version 7) and two-sample Kolmogorov-Smirnov test in Python. Outliers in behavioral analysis were removed after detection with Rosner's Extreme Studentized Deviate test. When performing multiple comparisons, p values were corrected using the Benjamini-Hochberg procedure. Differences were considered statistically significant if $p < 0.05$. Description of the number of animals used for each experiment and the number of neurons considered for each analysis can be found in the figure legends.

References

1. Rodrigues SM, LeDoux JE, Sapolsky RM. (2009). The influence of stress hormones on fear circuitry. *Annu. Rev. Neurosci.* 32, 289–313.
2. Li L, Feng X, Zhou Z, Zhang H, Shi Q, Lei Z, et al. (2018). Stress Accelerates Defensive Responses to Looming in Mice and Involves a Locus Coeruleus-Superior Colliculus Projection. *Curr. Biol.* 28, 859–871.
3. Evans DA, Stempel AV, Vale R, Branco T. (2019). Cognitive Control of Escape Behaviour. *Trends. Cogn. Sci.* 23, 334–348.
4. de Kloet ER, Joëls M, Holsboer F. (2005). Stress and the brain: from adaptation to disease. *Nat. Rev. Neurosci.* 6, 463–475.
5. Yehuda R, Hoge CW, McFarlane AC, Vermetten E, Lanius RA, Nievergelt CM, et al. (2015). Post-traumatic stress disorder. *Nat. Rev. Dis. Prim.* 1, 15057.
6. Chrousos GP. (2009) Stress and disorders of the stress system. *Nat. Rev. Endocrinol.* 5, 374–381.
7. Newport DJ, Nemeroff CB. (2000) Neurobiology of posttraumatic stress disorder. *Curr. Opin. Neurobiol.* 10, 211–218.
8. Ulrich-Lai YM, Herman JP. (2009) Neural regulation of endocrine and autonomic stress responses. *Nat. Rev. Neurosci.* 10, 397–409.
9. Herman JP, McKlveen JM, Ghosal S, Kopp B, Wulsin A, Makinson R, et al. (2016). Regulation of the Hypothalamic-Pituitary-Adrenocortical Stress Response. *Compr. Physiol.* 6, 603–621.
10. McEwen BS, Bowles NP, Gray JD, Hill MN, Hunter RG, Karatsoreos IN, et al. (2015). Mechanisms of stress in the brain. *Nat. Neurosci.* 18, 1353–1363.
11. Joëls M, Baram TZ. (2009). The neuro-symphony of stress. *Nat. Rev. Neurosci.* 10, 459–466.
12. Herman JP, Figueiredo H, Mueller NK, Ulrich-Lai YM, Ostrander MM, Choi DC, et al. (2003). Central mechanisms of stress integration: hierarchical circuitry controlling

- hypothalamo-pituitary-adrenocortical responsiveness. *Front. Neuroendocrinol.* 24, 151–180.
13. Kormos V, Gaszner B. (2013). Role of neuropeptides in anxiety, stress, and depression: from animals to humans. *Neuropeptides* 47, 401–419.
 14. Picciotto MR, Brabant C, Einstein EB, Kamens HM, Neugebauer NM. (2010). Effects of galanin on monoaminergic systems and HPA axis: Potential mechanisms underlying the effects of galanin on addiction- and stress-related behaviors. *Brain Res.* 1314, 206–218.
 15. Lang R, Gundlach AL, Holmes FE, Hobson SA, Wynick D, Hökfelt T, et al. (2015). Physiology, signaling, and pharmacology of galanin peptides and receptors: three decades of emerging diversity. *Pharmacol. Rev.* 67, 118–175.
 16. Portugues R, Severi KE, Wyart C, Ahrens MB. (2013). Optogenetics in a transparent animal: circuit function in the larval zebrafish. *Curr. Opin. Neurobiol.* 23, 119–126.
 17. Arrenberg AB, Driever W. (2013). Integrating anatomy and function for zebrafish circuit analysis. *Front. Neural Circuits* 7, 74.
 18. Baier H, Scott EK. (2009). Genetic and optical targeting of neural circuits and behavior-zebrafish in the spotlight. *Curr. Opin. Neurobiol.* 19, 553–560.
 19. Friedrich RW, Jacobson GA, Zhu P. (2010). Circuit neuroscience in zebrafish. *Curr. Biol.* 20, R371–381.
 20. Vanwallegheem GC, Ahrens MB, Scott EK. (2018). Integrative whole-brain neuroscience in larval zebrafish. *Curr. Opin. Neurobiol.* 50, 136–145.
 21. Löhr H, Hammerschmidt M. (2011). Zebrafish in endocrine systems: recent advances and implications for human disease. *Annu. Rev. Physiol.* 73, 183–211.
 22. Wendelaar Bonga SE. (1997). The stress response in fish. *Physiol. Rev.* 77, 591–625.
 23. Nagpal J, Herget U, Choi MK, Ryu S. (2019). Anatomy, development, and plasticity of the neurosecretory hypothalamus in zebrafish. *Cell Tissue Res.* 375, 5–22.

24. Ziv L, Muto A, Schoonheim PJ, Meijsing SH, Strasser D, Ingraham HA, et al. (2013). An affective disorder in zebrafish with mutation of the glucocorticoid receptor. *Mol. Psych.* 18, 681–691.
25. Berg-Maurer vom CM, Trivedi CA, Bollmann JH, De Marco RJ, Ryu S. (2016). The Severity of Acute Stress Is Represented by Increased Synchronous Activity and Recruitment of Hypothalamic CRH Neurons. *J. Neurosci.* 36, 3350–3362.
26. De Marco RJ, Thiemann T, Groneberg AH, Herget U, Ryu S. (2016). Optogenetically enhanced pituitary corticotroph cell activity post-stress onset causes rapid organizing effects on behaviour. *Nat. Commun.* 7, 12620.
27. Andalman AS, Burns VM, Lovett-Barron M, Broxton M, Poole B, Yang SJ, et al. (2019). Neuronal Dynamics Regulating Brain and Behavioral State Transitions. *Cell* 177, 970–985.
28. Förster D, Arnold-Ammer I, Laurell E, Barker AJ, Fernandes AM, Finger-Baier KC, et al. (2017). Genetic targeting and anatomical registration of neuronal populations in the zebrafish brain with a new set of BAC transgenic tools. *Sci. Rep.* 7: 5230
29. De Marco RJ, Groneberg AH, Yeh C-M, Treviño M, Ryu S. (2014). The behavior of larval zebrafish reveals stressor-mediated anorexia during early vertebrate development. *Front. Behav. Neurosci.* 8, 367.
30. Randlett O, Wee CL, Naumann EA, Nnaemeka O, Schoppik D, Fitzgerald JE, et al. (2015) Whole-brain activity mapping onto a zebrafish brain atlas. *Nat. Methods* 12, 1039–1046.
31. Ryu S, De Marco RJ. (2017). Performance on innate behaviour during early development as a function of stress level. *Sci. Rep.* 7, 7840.
32. Clark KJ, Boczek NJ, Ekker SC. (2011). Stressing zebrafish for behavioral genetics. *Rev. Neurosci.* 22, 49–62.
33. Pisharath H, Rhee JM, Swanson MA, Leach SD, Parsons MJ. (2007). Targeted ablation of beta cells in the embryonic zebrafish pancreas using *E. coli* nitroreductase. *Mech. Dev.* 124, 218–229.

34. Bergemann D, Massoz L, Bourdouxhe J, Carril Pardo CA, Voz ML, Peers B, et al. Nifurpirinol: (2018). A more potent and reliable substrate compared to metronidazole for nitroreductase-mediated cell ablations. *Wound Repair Regen.* 26, 238–244.
35. Grillon C, Baas J. (2003). A review of the modulation of the startle reflex by affective states and its application in psychiatry. *Clin. Neurophysiol.* 114, 1557–1579.
36. Griffiths BB, Schoonheim PJ, Ziv L, Voelker L, Baier H, Gahtan E. (2012). A zebrafish model of glucocorticoid resistance shows serotonergic modulation of the stress response. *Front. Behav. Neurosci.* 6: 68.
37. Ray WJ, Molnar C, Aikins D, Yamasaki A, Newman MG, Castonguay L, et al. (2009). Startle response in generalized anxiety disorder. *Depress. Anxiety* 26, 147–154.
38. Wu Z, Autry AE, Bergan JF, Watabe-Uchida M, Dulac CG. (2014). Galanin neurons in the medial preoptic area govern parental behaviour. *Nature* 509, 325–330.
39. Choi HMT, Schwarzkopf M, Fornace ME, Acharya A, Artavanis G, Stegmaier J, et al. (2018). Third-generation in situ hybridization chain reaction: multiplexed, quantitative, sensitive, versatile, robust. *Development* 145, dev165753.
40. Schick RR, Samsami S, Zimmermann JP, Eberl T, Endres C, Schusdziarra V, et al. (1993). Effect of galanin on food intake in rats: involvement of lateral and ventromedial hypothalamic sites. *Am. J. Physiol.* 264, R355–61.
41. Leibowitz SF, Akabayashi A, Wang J. (1998). Obesity on a high-fat diet: role of hypothalamic galanin in neurons of the anterior paraventricular nucleus projecting to the median eminence. *J. Neurosci.* 18, 2709–2719.
42. Adams AC, Clapham JC, Wynick D, Speakman JR. (2008). Feeding behaviour in galanin knockout mice supports a role of galanin in fat intake and preference. *J Neuroendocrinol.* 20, 199–206.
43. Laque A, Yu S, Qualls-Creekmore E, Gettys S, Schwartzburg C, Bui K, et al. (2015). Leptin modulates nutrient reward via inhibitory galanin action on orexin neurons. *Mol. Metab.* 4, 706–717.

44. Qualls-Creekmore E, Yu S, Francois M, Hoang J, Huesing C, Bruce-Keller A, et al. (2017). Galanin-Expressing GABA Neurons in the Lateral Hypothalamus Modulate Food Reward and Noncompulsive Locomotion. *J. Neurosci.* 37, 6053–6065.
45. Kohl J, Babayan BM, Rubinstein ND, Autry AE, Marin-Rodriguez B, Kapoor V, et al. (2018). Functional circuit architecture underlying parental behaviour. *Nature* 556, 326–331.
46. Chen S, Reichert S, Singh C, Oikonomou G, Rihel J, Prober DA. (2017). Light-Dependent Regulation of Sleep and Wake States by Prokineticin 2 in Zebrafish. *Neuron* 95, 153–168.
47. Reichert S, Pavón Arocas O, Rihel J. (2019). The Neuropeptide Galanin Is Required for Homeostatic Rebound Sleep following Increased Neuronal Activity. *Neuron* 104, 370–384.
48. Van Reeth O, Weibel L, Spiegel K, Reproult R, Dugovic C, Maccari S. (2000). Physiology of sleep (review)—interactions between stress and sleep: from basic research to clinical situations. *Sleep Medicine Reviews* 4(2), 201–219.
49. Herrera KJ, Panier T, Guggiana-Nilo D, Engert F. (2021) Larval Zebrafish Use Olfactory Detection of Sodium and Chloride to Avoid Salt Water. *Curr. Biol.* 31:782–793.
50. Tillage RP, Wilson GE, Liles LC, Holmes PV, Weinshenker D. (2020). Chronic Environmental or Genetic Elevation of Galanin in Noradrenergic Neurons Confers Stress Resilience in Mice. *J. Neurosci.* 40, 7464–7474.
51. Tillage RP, Foster SL, Lustberg D, Liles LC, McCann KE, Weinshenker D. (2021). Co-released norepinephrine and galanin act on different timescales to promote stress-induced anxiety-like behavior. *Neuropsychopharmacology* 46, 1535–1543.
52. Pieribone VA, Xu ZQ, Zhang X, Grillner S, Bartfai T, Hokfelt T. (1995). Galanin induces a hyperpolarization of norepinephrine-containing locus coeruleus neurons in the brainstem slice. *Neuroscience* 64, 861–874.

53. Zini S, Roisin MP, Langel U, Bartfai T, Ben-Ari Y. (1993). Galanin reduces release of endogenous excitatory amino acids in the rat hippocampus. *Europ. J. Pharmacol.* 245, 1–7.
54. Kozoriz MG, Kuzmiski JB, Hirasawa M, Pittman QJ. (2006). Galanin modulates neuronal and synaptic properties in the rat supraoptic nucleus in a use and state dependent manner. *J. Neurophysiol.* 96, 154–164.
55. Ma X, Tong YG, Schmidt R, Brown W, Payza K, Hodzic L, et al. (2001). Effects of galanin receptor agonists on locus coeruleus neurons. *Brain Res.* 919, 169–174.
56. Kinney GA, Emmerson PJ, Miller RJ. (1998). Galanin receptor-mediated inhibition of glutamate release in the arcuate nucleus of the hypothalamus. *J. Neurosci.* 18, 3489–3500.
57. Asakawa K, Suster ML, Mizusawa K, Nagayoshi S, Kotani T, Urasaki A, et al. (2008). Genetic dissection of neural circuits by Tol2 transposon-mediated Gal4 gene and enhancer trapping in zebrafish. *Proc. Natl. Acad. Sci. USA* 105, 1255–1260.
58. Davison JM, Akitake CM, Goll MG, Rhee JM, Gosse N, Baier H, et al. (2007). Transactivation from Gal4-VP16 transgenic insertions for tissue-specific cell labeling and ablation in zebrafish. *Dev. Biol.* 304, 811–824.
59. Thiele TR, Donovan JC, Baier H. (2014). Descending control of swim posture by a midbrain nucleus in zebrafish. *Neuron* 83, 679–691.
60. Freeman J, Vladimirov N, Kawashima T, Mu Y, Sofroniew NJ, Bennett DV, et al. (2014). Mapping brain activity at scale with cluster computing. *Nat. Methods* 11:941–50.
61. Filosa A, Barker AJ, Dal Maschio M, Baier H. (2016). Feeding State Modulates Behavioral Choice and Processing of Prey Stimuli in the Zebrafish Tectum. *Neuron* 90, 596–608.
62. Thisse C, Thisse B. (2008). High-resolution in situ hybridization to whole-mount zebrafish embryos. *Nat. Prot.* 3(1):59-69

63. Podlasz P, Sallinen V, Chen YC, Kudo H, Fedorowska N, Panula P. (2012). Galanin gene expression and effects of its knock-down on the development of the nervous system in larval zebrafish. *J. Comp. Neurol.* 520:3846-3862.
64. Lister JA, Robertson CP, Lepage T, Johnson SL, Raible DW. (1999). nacre encodes a zebrafish microphthalmia-related protein that regulates neural-crest-derived pigment cell fate. *Development* 126, 3757–67.
65. Pnevmatikakis EA, Giovannucci A. (2017) NoRMCorre: An online algorithm for piecewise rigid motion correction of calcium imaging data. *J. Neurosci. Methods.* 291:83-94.
66. Deneux T, Kaszas A, Szalay G, Katona G, Lakner T, Grinvald A, et al. (2016). Accurate spike estimation from noisy calcium signals for ultrafast three-dimensional imaging of large neuronal populations in vivo. *Nat. Commun.* 7:12190.
67. Bruzzone M, Chiarello E, Albanesi M, Miletto Petrazzini ME, Megighian A, Lodovichi C, et al. (2021). Whole brain functional recordings at cellular resolution in zebrafish larvae with 3D scanning multiphoton microscopy. *Sci. Rep.* 11:11048
68. Avants BB, Tustison NJ, Song G, (2009). Advanced normalization tools (ANTS)." *Insight j* 2.365: 1-35.
69. Kunst M, Laurell E, Mokayes N, Kramer A, Kubo F, Fernandes AM, et al. (2019). A Cellular-Resolution Atlas of the Larval Zebrafish Brain. *Neuron* 103:21–5.
70. Yeh C-M, Glöck M, Ryu S. (2013). An Optimized Whole-Body Cortisol Quantification Method for Assessing Stress Levels in Larval Zebrafish. *PLoS ONE* 8, e79406.

Figure 1

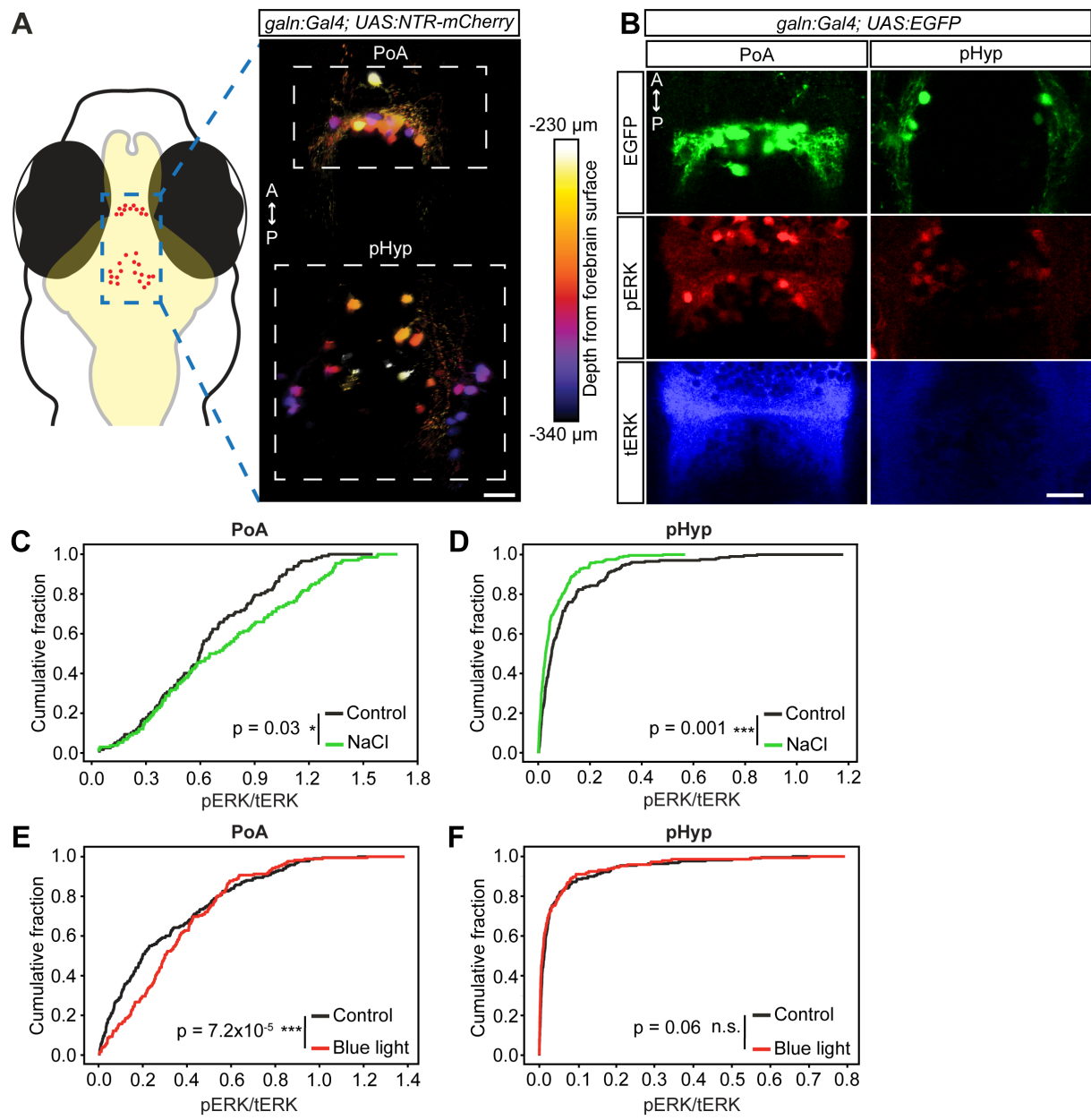


Figure 2

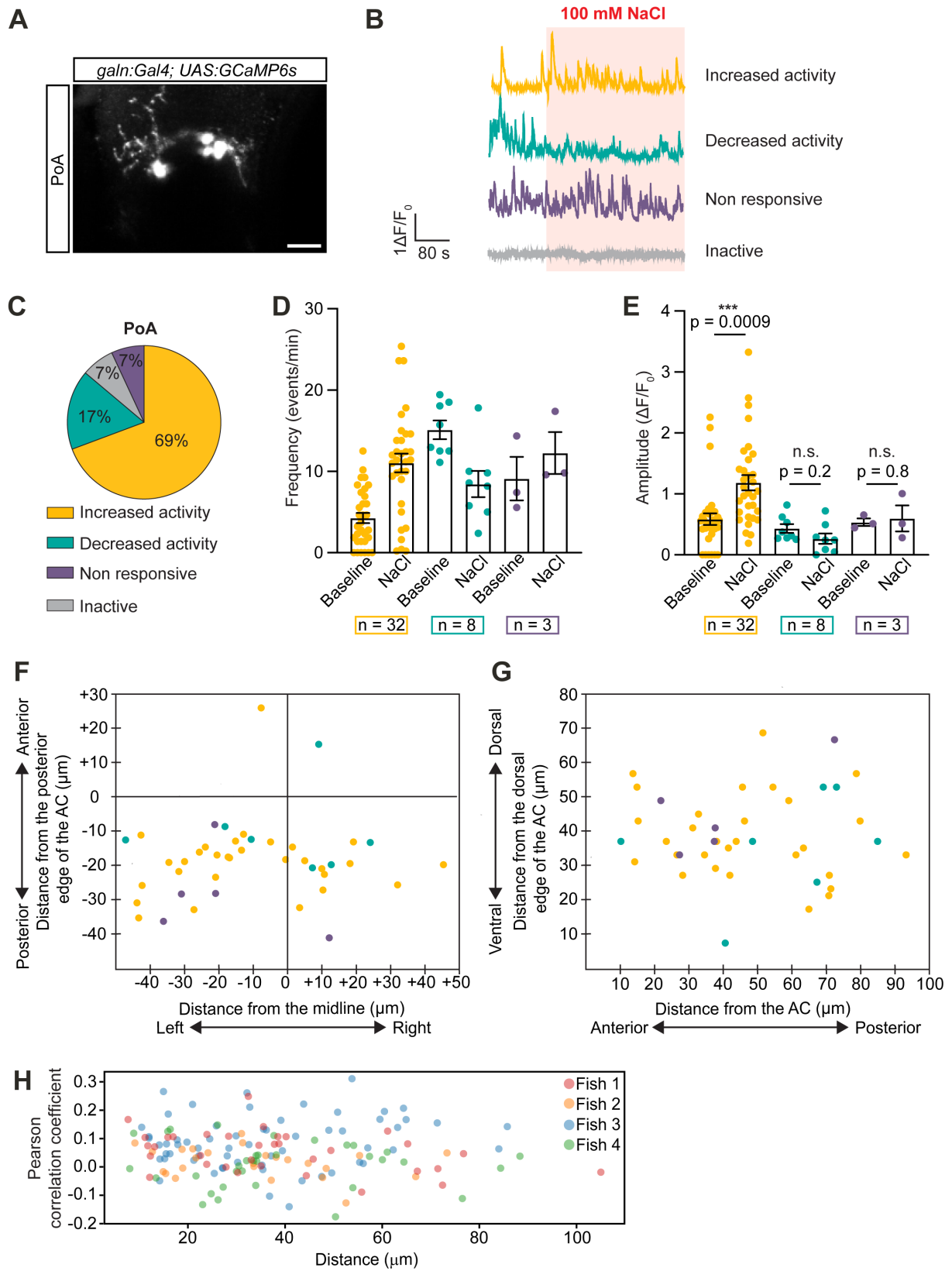


Figure 3

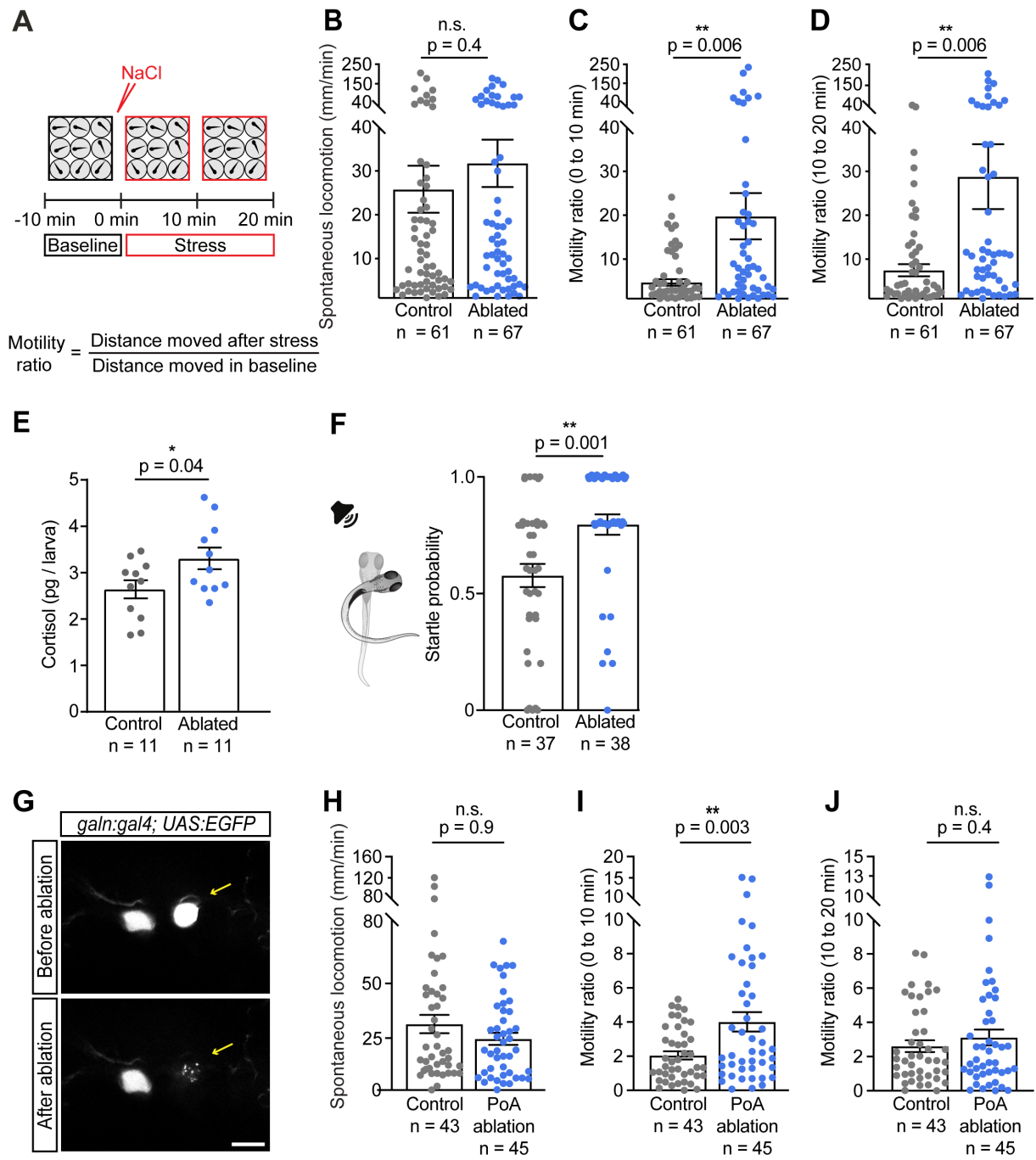


Figure 4

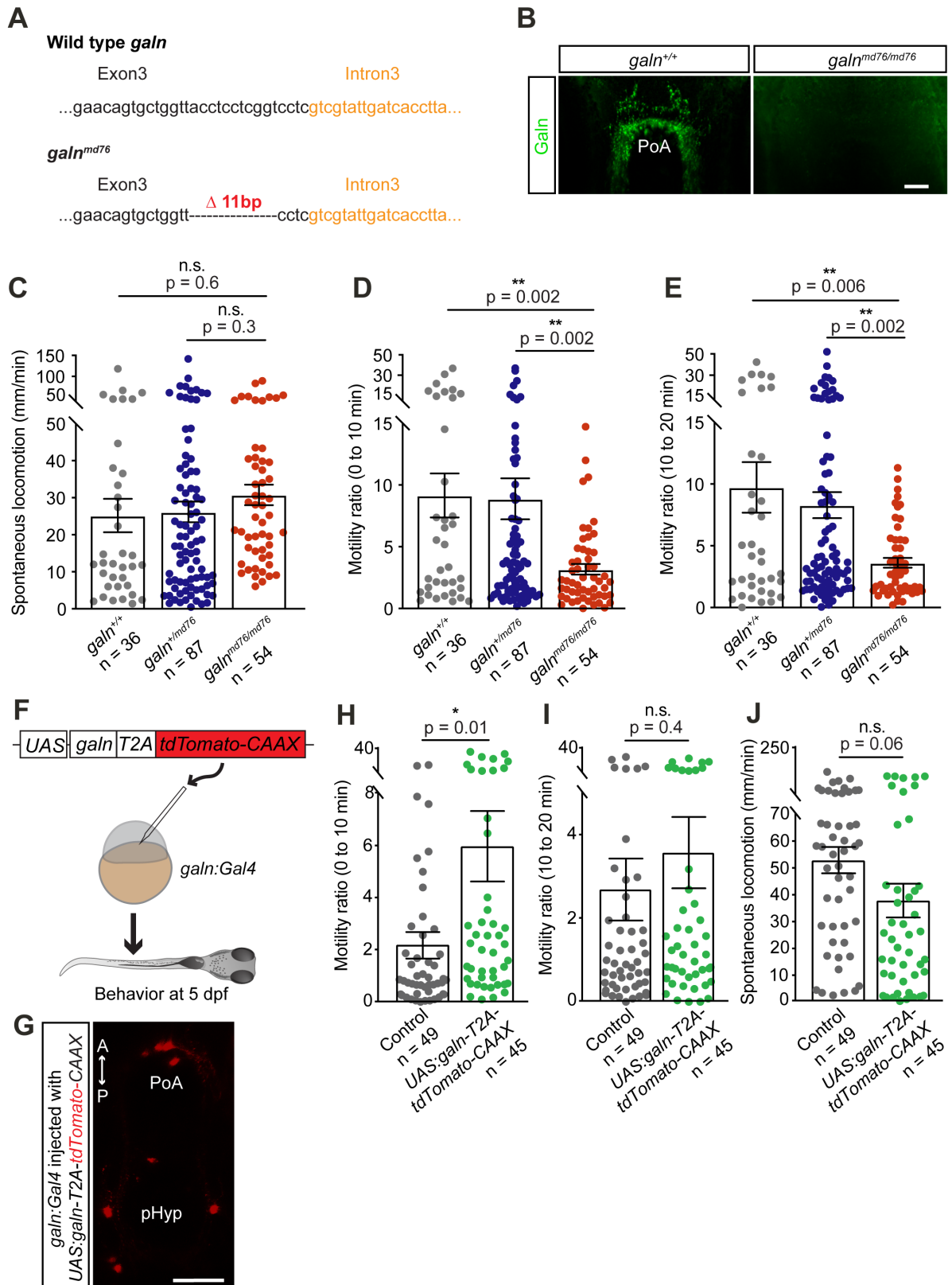


Figure 5

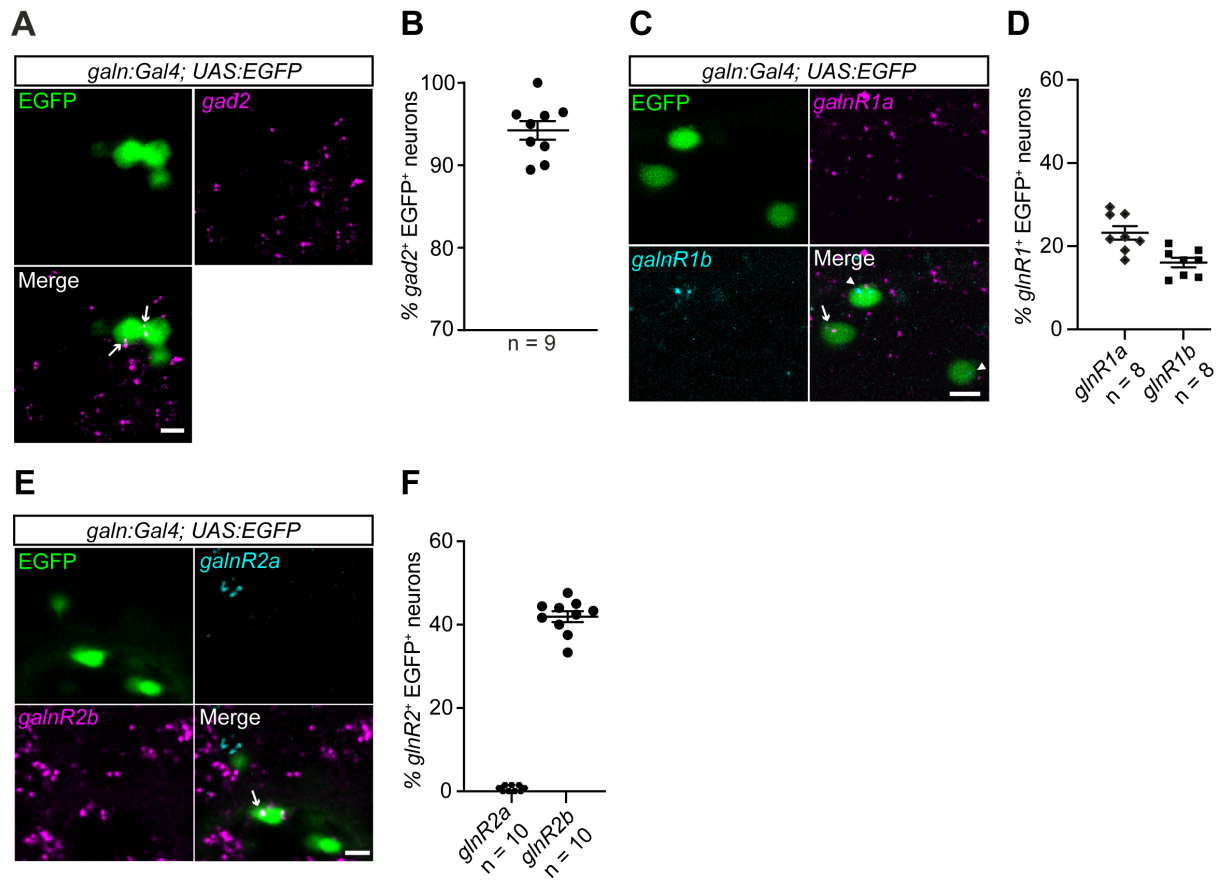


Figure 6

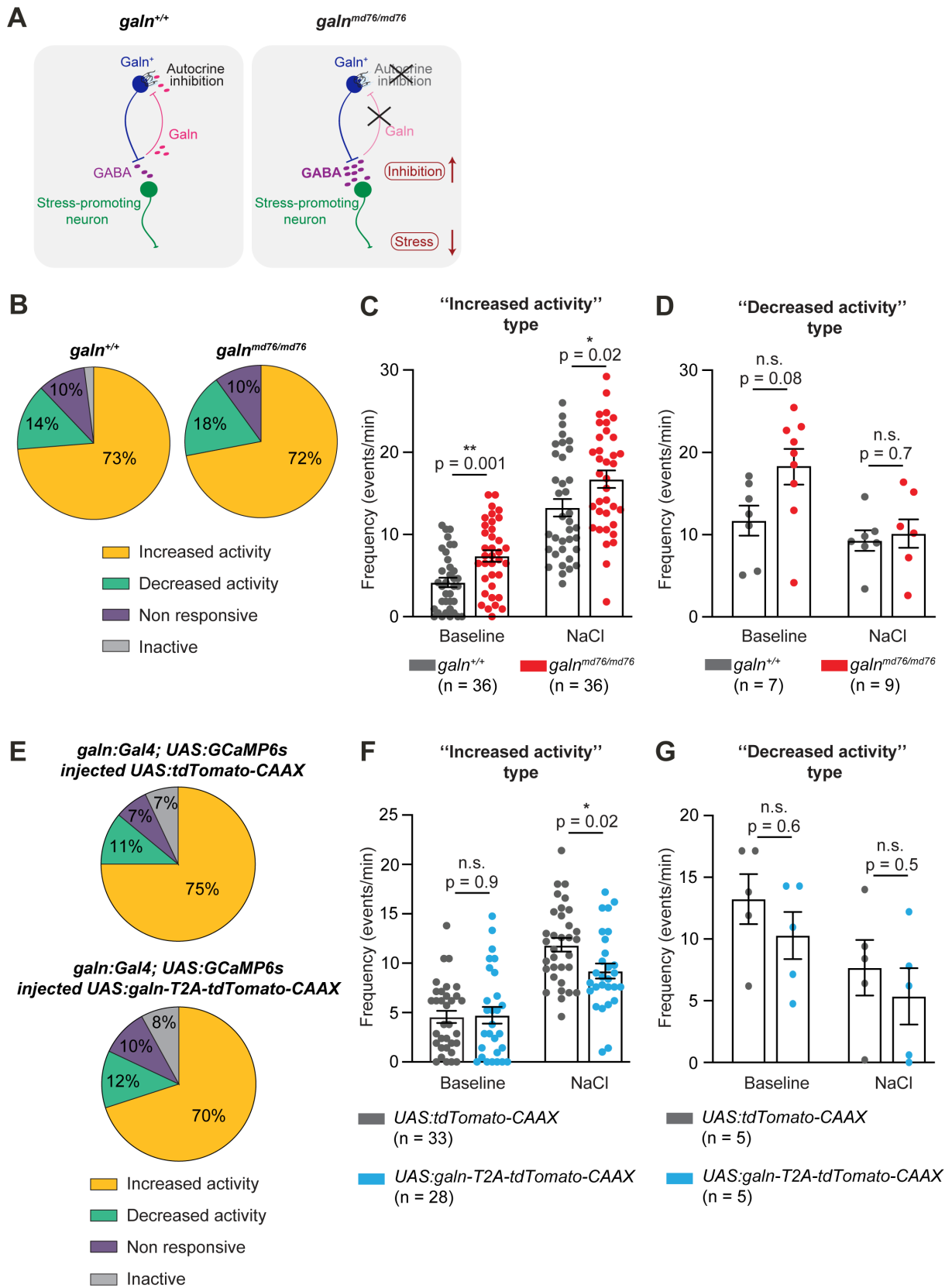
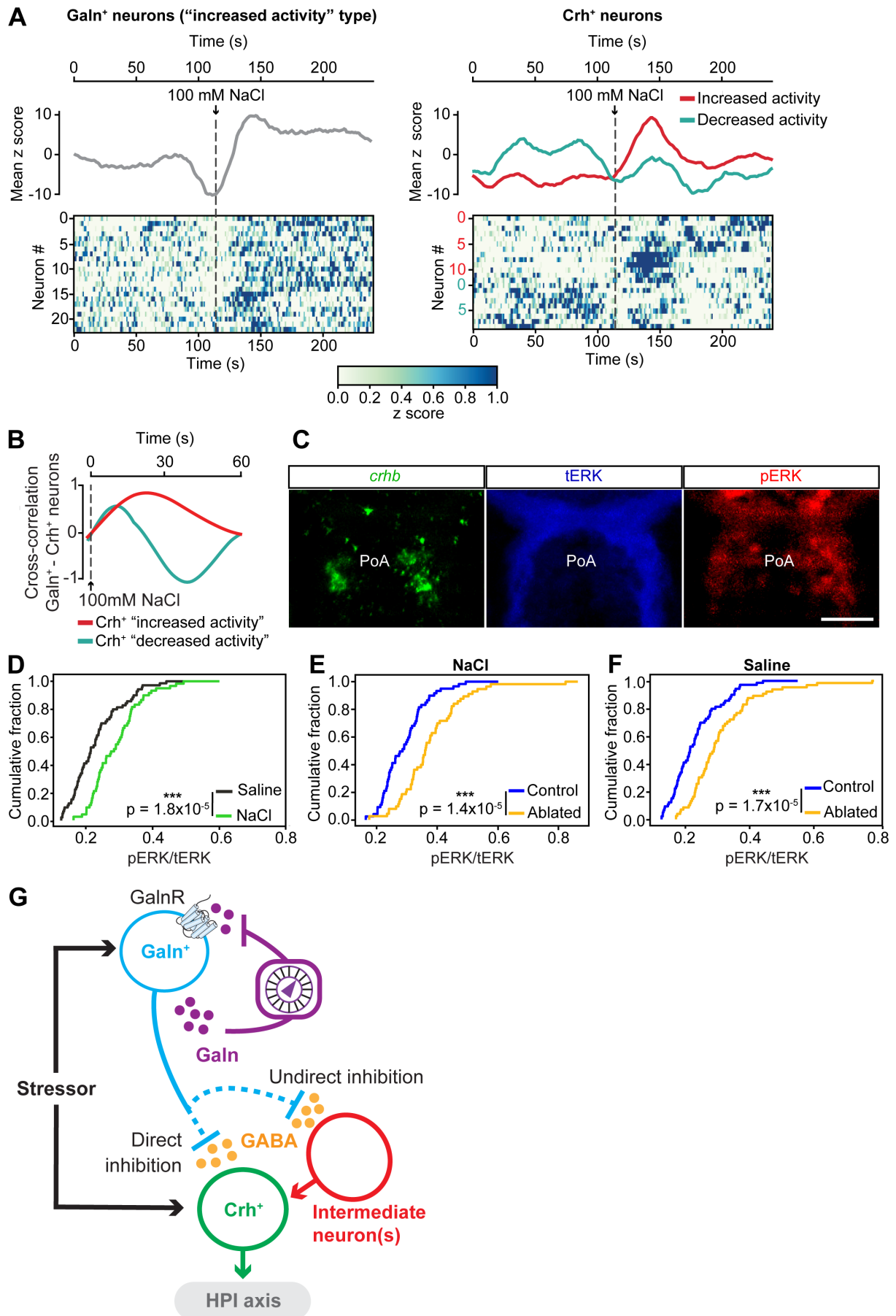


Figure 7



Supplemental Figures

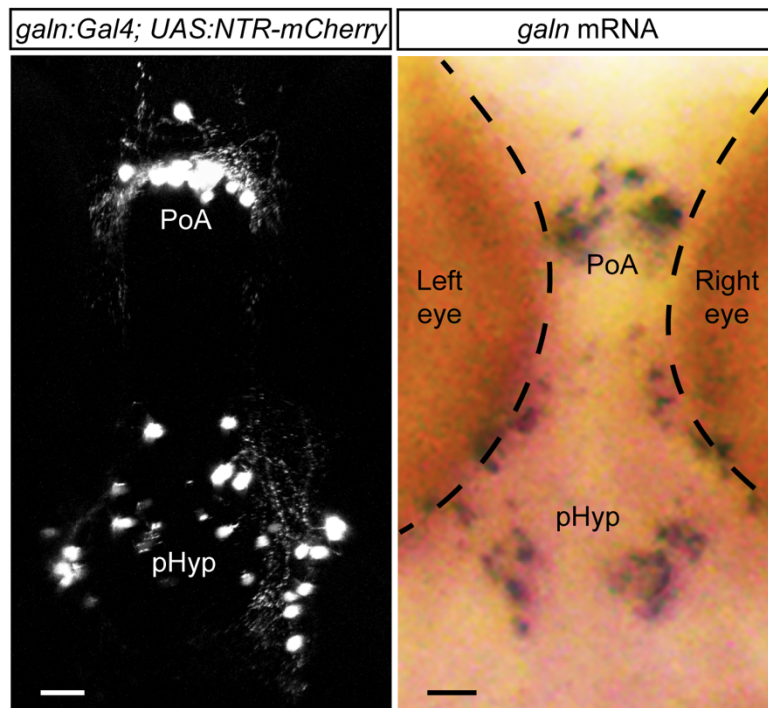


Figure S1 (related to Figure 1). The *galn:Gal4* transgenic line recapitulates expression of the *galn* gene. Left: maximum projection of a confocal stack showing Galn⁺ neurons in a 5 dpf *galn:Gal4; UAS:NTR-mCherry* larva (the image is also displayed in Figure 1A, in which depth of the neurons is color-coded). Right: image of the brain of a 5 dpf wild type larva after *in situ* hybridization to detect *galn* mRNA (in purple). Scale bars = 25 μ m.

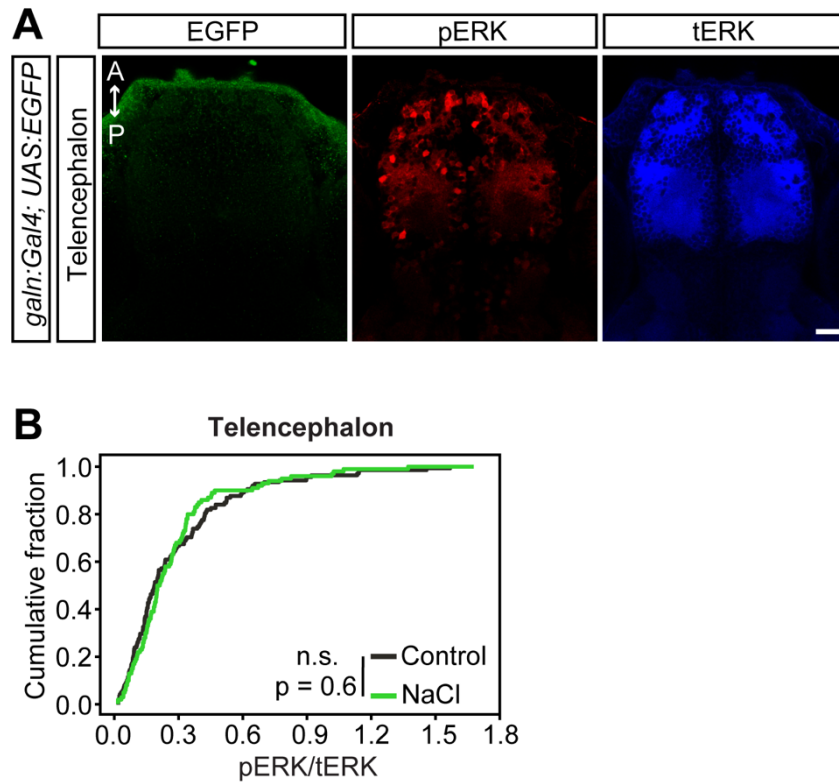


Figure S2 (related to Figure 1). Neuronal activity of Galn-negative neurons in the forebrain is not altered by hyperosmotic stress. A. Confocal images of the telencephalon of a 5 dpf *galn:Gal4; UAS:EGFP* larva immunostained with antibodies against GFP, pERK, and tERK. A and P indicate anterior and posterior directions respectively. Scale bar = 25 μ m. **B.** Graph depicting cumulative fractions of pERK/tERK values in randomly selected telencephalic Galn-negative neurons in 5 dpf *galn:Gal4; UAS:EGFP* larvae. $n_{\text{control}} = 138$ neurons from 7 larvae, $n_{\text{NaCl}} = 100$ neurons from 7 larvae. n.s. = not significant, two-sample Kolmogorov-Smirnov test.

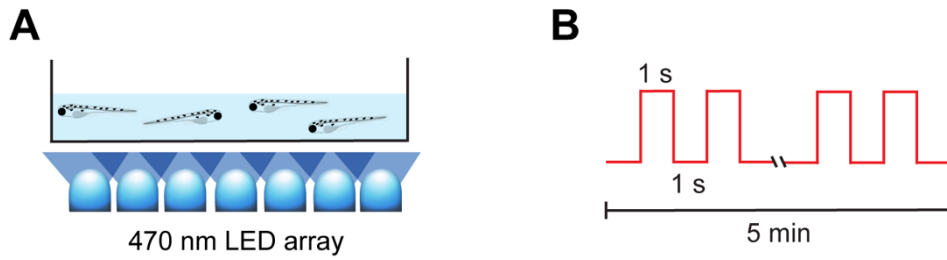


Figure S3 (related to Figure 1). Light-induced stress in zebrafish larvae. A. Schematic representation of the setup used to induce stress in zebrafish larvae with intense blue light. 5 dpf zebrafish larvae freely swimming in a Petri dish were irradiated with 470 nm light emitted from below by a LED array. **B.** Scheme of the light-exposure protocol. One-second-long pulses of light, with an inter-pulse interval of one second, were applied for five minutes.

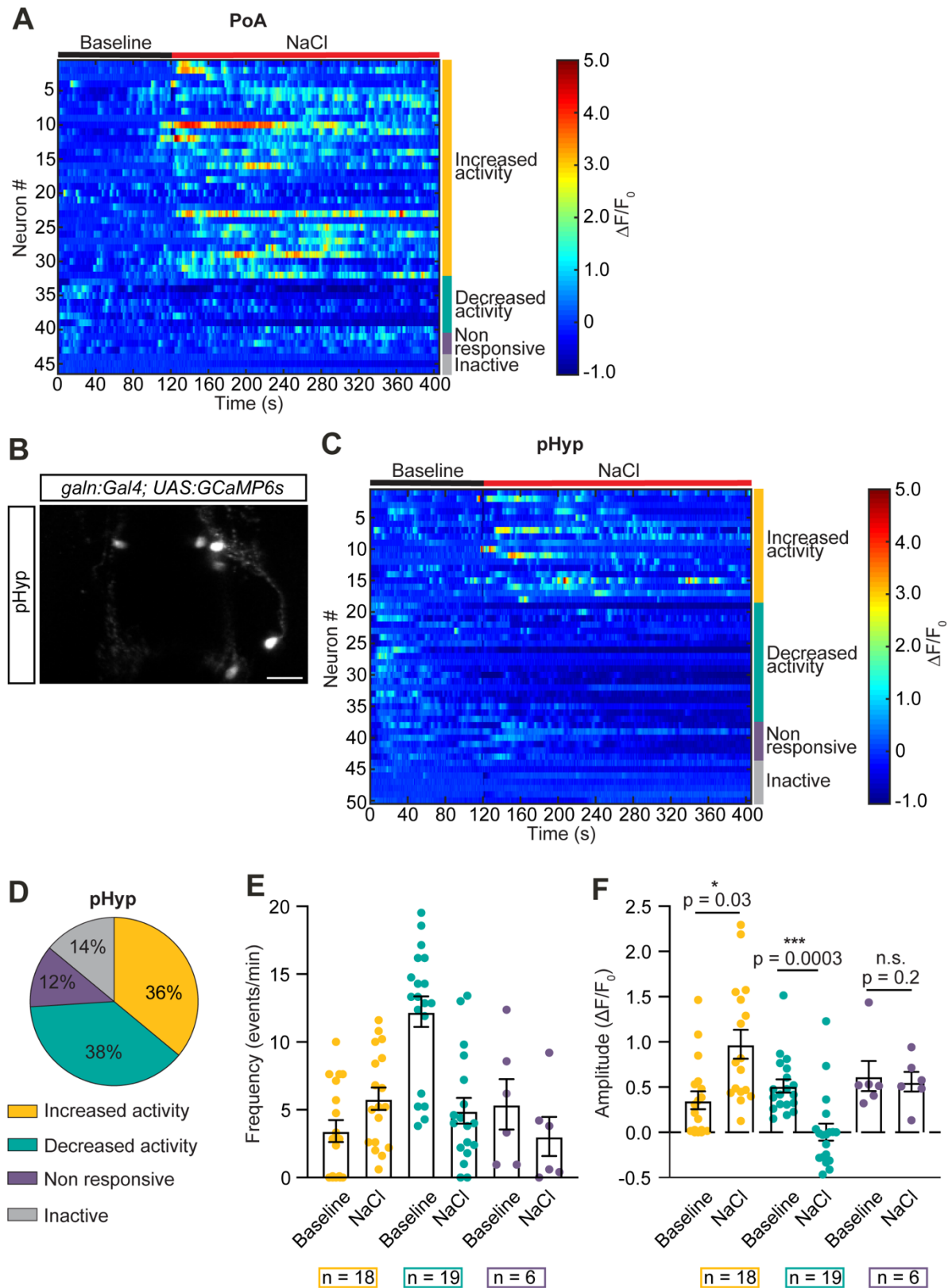


Figure S4 (related to Figure 2). Subtypes of Galn⁺ neurons display different responses to a stressor. A. Raster plot depicting $\Delta F/F_0$ values of the Galn⁺ neurons recorded in the PoA. **B.** Image showing Galn⁺/GCaMP6s⁺ neurons in the pHyp of a 5 dpf *galn:Gal4; UAS:GCaMP6s*

larva. Scale bar = 25 μm . **C.** Raster plot showing $\Delta F/F_0$ values of the Galn^+ neurons recorded in the pHyp. **D.** Pie chart showing percentages of response types of Galn^+ neurons in the pHyp. **E, F.** Graphs displaying average frequency (E) and amplitude (F) of calcium transients in Galn^+ neurons in the pHyp before (baseline) and after (NaCl) exposure to the hypertonic solution. Color coding as in (D). In (C – F) data were obtained from 10 (increased activity group), 16 (decreased activity group), 6 (non responsive group), and 7 (inactive group) larvae. Data are shown as mean \pm SEM. n = number of neurons. * $p < 0.05$, *** $p < 0.001$, n.s. = not significant, two-tailed t-test. Statistical tests were not performed in (E) because frequency was already used as a parameter for classification of neuronal types.

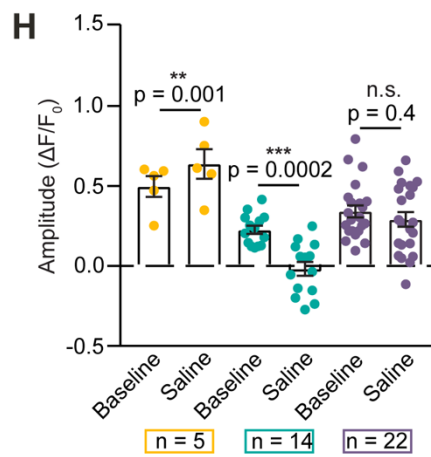
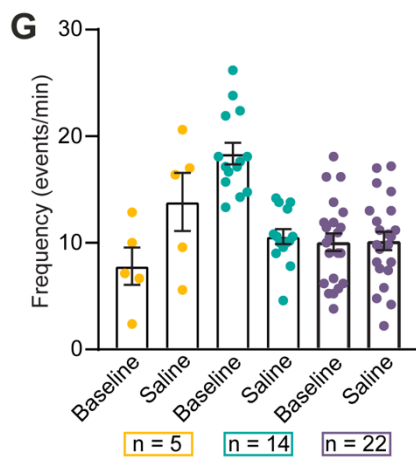
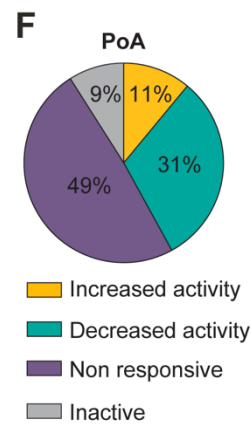
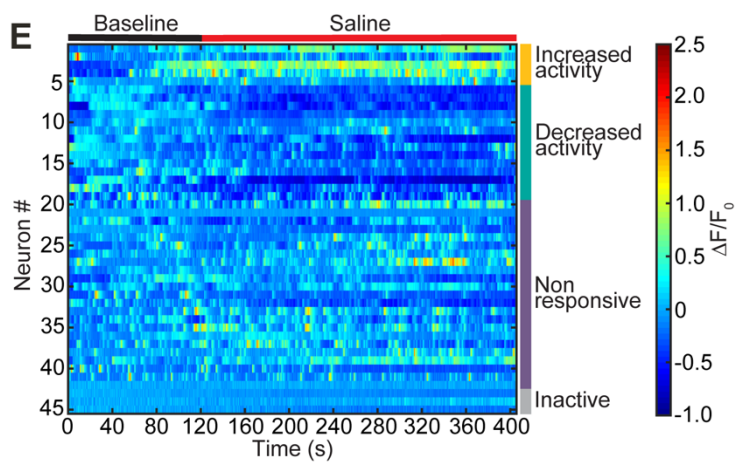
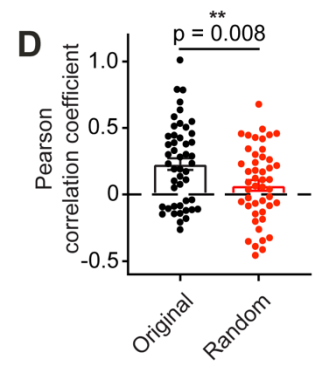
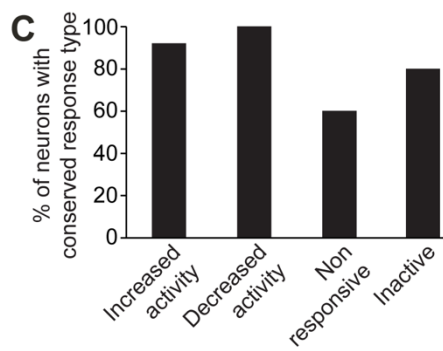
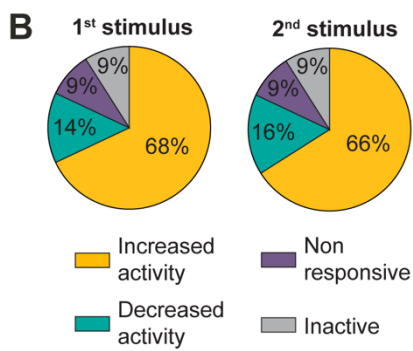
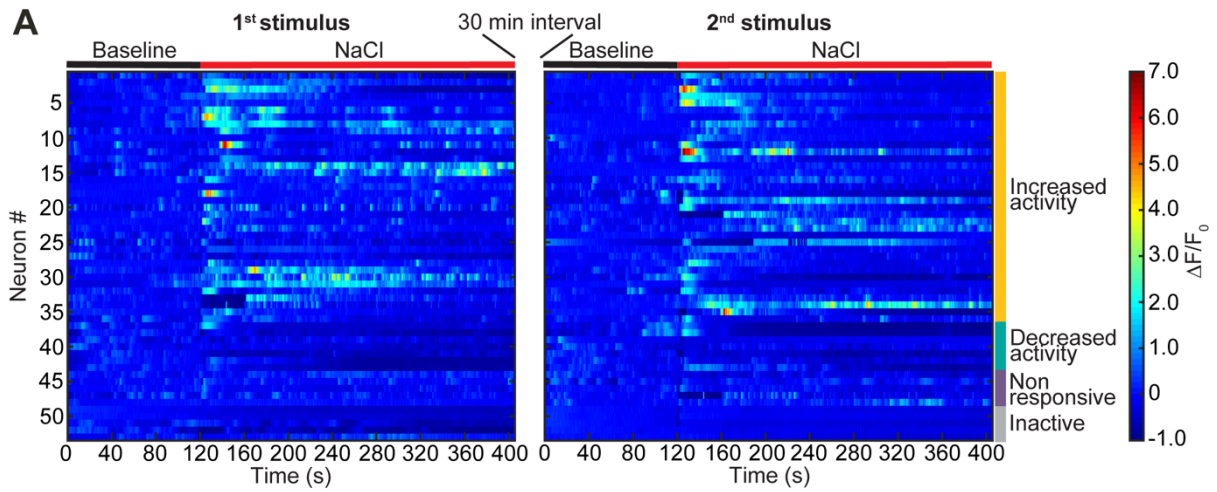


Figure S5 (related to Figure 2). Responses of Galn⁺ neurons in the PoA to consecutive applications of the hypertonic solution, or saline solution. A. Raster plots depicting $\Delta F/F_0$ values of the Galn⁺ neurons recorded in the PoA of 5dpf *galn:Gal4; UAS:GCaMP6s* larvae during two consecutive application of the 100 mM NaCl solution. **B.** Pie charts showing similar percentages of the four classes of Galn⁺ neurons in the PoA after the first and second stimulation. **C.** Bar graph showing percentages of neurons with conserved response types in the second stimulation compared to the first one. **D.** Graph depicting Pearson correlation coefficients of neuronal activity of Galn⁺ neurons during the first and second stimulations (original), or of randomly matched neurons across trials (random). In (A – D) data were obtained from 20 (increased activity group), 5 (decreased activity group), 5 (non responsive group), and 3 (inactive group) larvae. **E.** Raster plot showing $\Delta F/F_0$ values of the Galn⁺ neurons recorded in the PoA of 5 dpf *galn:Gal4; UAS:GCaMP6s* larvae during application of a saline (Danieau's) solution. **F.** Pie chart illustrating percentages of the four types of Galn⁺ neurons in the PoA after application of the saline solution. **G, H.** Bar graphs showing average frequency (G) and amplitude (H) of calcium transients in Galn⁺ neurons in the PoA before (baseline) and after (saline) exposure to the saline solution. Color coding as in (B, F). In (E – H) data were obtained from 5 (increased activity group), 11 (decreased activity group), 19 (non responsive group), 4 (inactive group) larvae. Data in (D), (G), and (H) are shown as mean \pm SEM. n = number of neurons. ** p < 0.01, *** p < 0.001, n.s. = not significant, two-tailed t-test. Statistical tests were not performed in (G) because frequency was already used as a parameter for classification of neuronal types.

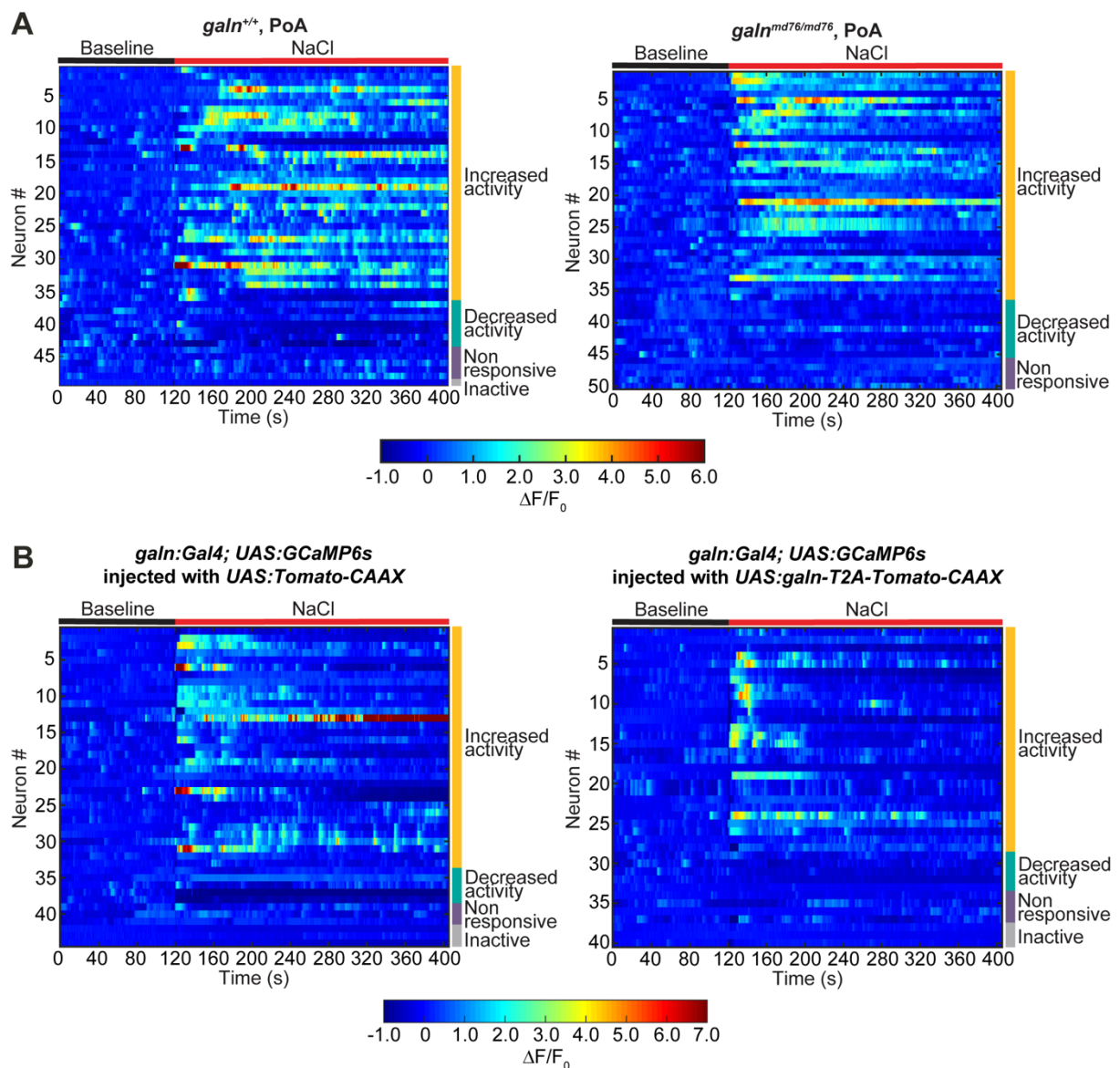


Figure S6 (related to Figure 6). Responses of Galn⁺ neurons in the PoA of fish lacking or overexpressing *galn*. **A, B.** Raster plots depicting $\Delta F/F_0$ values of the Galn⁺ neurons in the PoA of 5 dpf *galn:Gal4; UAS:GCaMP6s; galn^{+/+}* and *galn:Gal4; UAS:GCaMP6s; galn^{md76/md76}* larvae (A), or 5 dpf *galn:Gal4; UAS:GCaMP6s* fish injected with *UAS:tdTomato-CAAX* or *UAS:galn-T2A-tdTomato-CAAX* constructs (B).

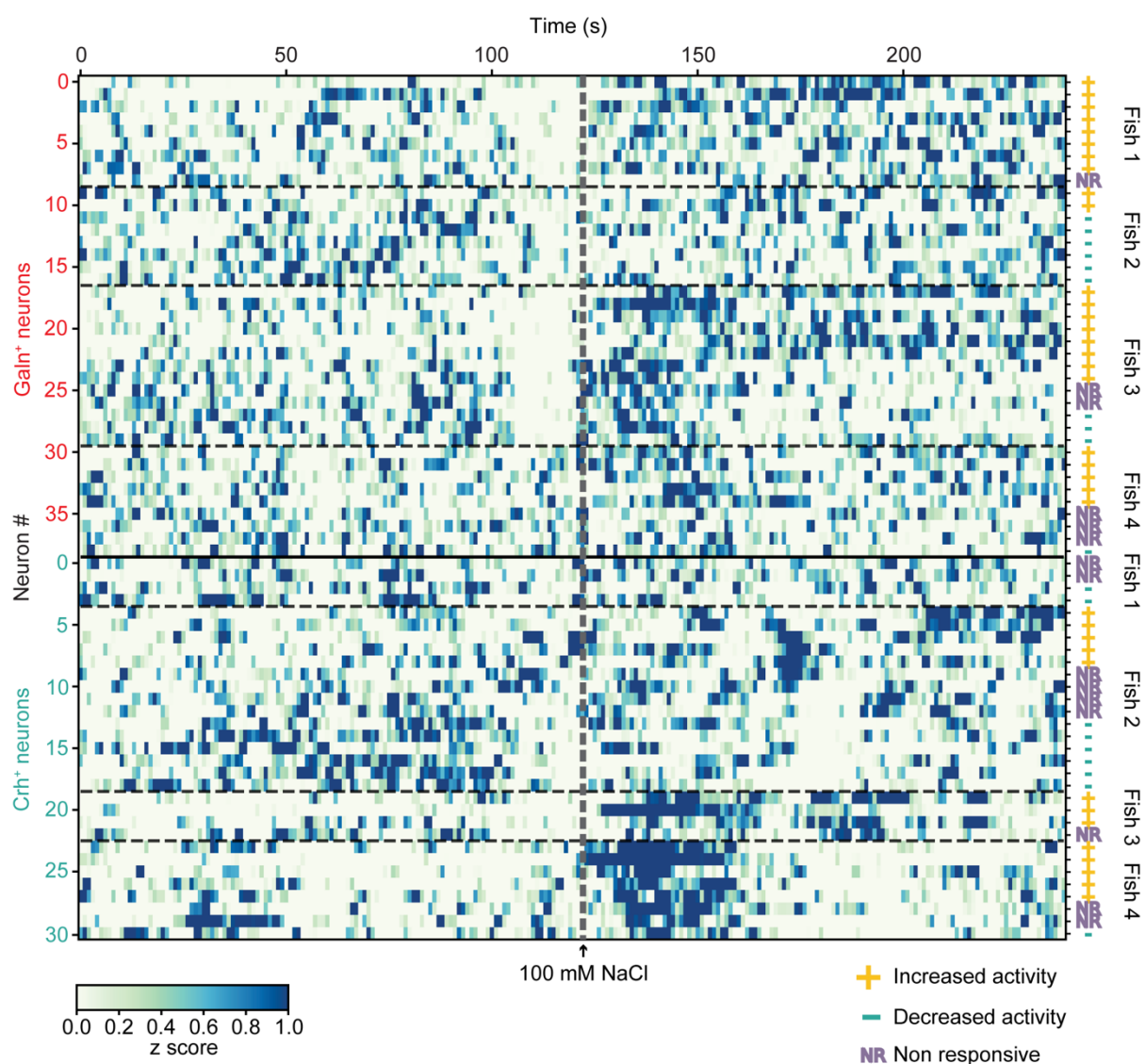


Figure S7 (related to Figure 7). Stressor-induced activity of Galn⁺ and Crh⁺ neurons.

Raster plot displaying activity (z scores) of Galn⁺ and Crh⁺ neurons in the PoA of four 5 dpf *galn:Gal4; UAS:NTR-mCherry; elavl3:H2B-GCaMP6s* larvae before and after exposure to 100 mM NaCl solution. Crh⁺ neurons were identified post mortem with *in situ* hybridization (see Star Methods). The type of stressor-induced response for each neuron—“increased activity” (+), “decreased activity” (-), and non responsive (NR)—is indicated on the right side of the plot. To enhance neuronal activity visualization, the scale of the color bar was adjusted by narrowing the range to 0–1.